water

Article

A Holocene Sedimentary Record and the Impact of Sea-Level Rise in the Karst Lake Velo Blato and the Wetlands on Pag Island (Croatia)

Nikolina Ilijanić [1,*], Slobodan Miko [1], Ivona Ivkić Filipović [1], Ozren Hasan [1], Martina Šparica Miko [1], Branko Petrinec [2], Josip Terzić [1] and Tamara Marković [1]

[1] Croatian Geological Survey, Sachsova 2, 10000 Zagreb, Croatia; smiko@hgi-cgs.hr (S.M.); iivkic@hgi-cgs.hr (I.I.F.); ohasan@hgi-cgs.hr (O.H.); mtsparica@hgi-cgs.hr (M.Š.M.); jterzic@hgi-cgs.hr (J.T.); tmarkovic@hgi-cgs.hr (T.M.)
[2] Institute for Medical Research and Occupational Health, Ksaverska cesta 2, 10001 Zagreb, Croatia; petrinec@imi.hr
* Correspondence: nilijanic@hgi-cgs.hr

Abstract: Lakes in coastal lowland areas represent a critically vulnerable environment as a transitional space between freshwater and seawater environments. The paleoenvironmental reconstruction and anthropogenic impact are assessed through the lake sediment cores from Velo, Malo, and Kolanjsko Blato using multi-proxy analyses (sedimentological, mineralogical, geochemical, ^{137}Cs and ostracod analyses, and AMS ^{14}C radiocarbon dating). The freshwater lake Velo Blato was formed at 8100 cal yr BP due to rising groundwater levels as a consequence of sea-level rise. The brackish conditions in Lake Velo Blato started at 7100 cal yr BP, giving the index point for the sea-level curve of 7-m lower than present. Lead concentrations showed slightly increased values in the last 1800 cal yr BP, while the spike in Malo Blato lake sediments probably derived from bird hunting with lead bullets. Kolanjsko Blato sediment core archives the sediment record of the last 2050 years, which represents a shallow brackish coastal wetland under marine influence. Enrichment factors showed the accumulation of Cu, Hg, P, Pb, S, and Zn in the sediments from Kolanjsko Blato in the last 650 cal yr BP, which coincides with the high organic carbon content, and in sediments from Malo Blato after the lake's formation (from the depth of 20 cm upwards). Anthropogenic Cu introduced into the Kolanjsko Blato sediments is the highest in the surface sample. Surficial sediments from Velo Blato are characterized by the high organic carbon, S, P, and N content, indicating high productivity and eutrophication which led to occasional anoxic conditions on the lake bottom in the last 200 years.

Keywords: coastal lake and wetlands; lake sediments; karst; eastern Adriatic coast; geochemistry; heavy metals; total organic carbon; ostracods

Citation: Ilijanić, N.; Miko, S.; Ivkić Filipović, I.; Hasan, O.; Šparica Miko, M.; Petrinec, B.; Terzić, J.; Marković, T. A Holocene Sedimentary Record and the Impact of Sea-Level Rise in the Karst Lake Velo Blato and the Wetlands on Pag Island (Croatia). *Water* **2022**, *14*, 342. https://doi.org/10.3390/w14030342

Academic Editor: Lu Zhang

Received: 23 December 2021
Accepted: 18 January 2022
Published: 24 January 2022

1. Introduction

The low-lying coastal areas in the Mediterranean, such as the eastern Adriatic coast (EAC), are under constant threat of marine influence during Holocene transgression, i.e., relative sea-level (RSL) rise. A fluctuating sea level generates changes in coastal areas due to the increase in salinity. The lake–wetland systems in coastal areas are especially vulnerable in this context. This paper tries to determine whether this is due to human anthropogenic activities (industry, urbanization, tourism, and food production) or naturally occurring environmental changes. The sedimentary lake record presents a valuable archive to identify this impact in the past and to reconstruct the trends for future changes. Lake sediments have been widely used as environmental indicators [1], and they can record Late Quaternary paleoclimate changes and hydrology, but they also reflect local, catchment-specific processes, evidenced across the Mediterranean lakes [2]. Holocene climate variability is generally weaker in amplitude than the climate fluctuations of the last glacial interval; therefore, high-resolution multi-proxy records are essential [3,4]. In karst areas, most of the Quaternary deposits are not preserved due to the nature of karst and its porous features and high permeability [5]. Compared to rivers and streams, lake wetlands may seem like peaceful unchanging environments, but they undergo physical changes at spatial and temporal scales, especially under marine influence. Changes in vegetation, lake levels, and seawater impacts may greatly influence wetland biota. Coastal wetlands are defined as ecosystems found within an elevation gradient that ranges between subtidal depths, at which light penetrates to support photosynthesis of benthic plants, and the landward edge, where the sea passes its hydrologic influence to groundwater and atmospheric processes [6]. Coastal lakes and wetlands are transitional ecosystems between land, freshwater, and seawater. In addition, the Croatian karstic coast is scant in terms of permanent freshwater body occurrences; most of the basins drowned from the period of the Last Glacial Maximum (LGM) lowstand to the Holocene sea-level rise, well-known along the EAC [7]. Therefore, karst, near the sea, has generally evolved in response to Quaternary sea-level changes. The recent EAC has been shaped by the last (Late Pleistocene–Holocene) sea-level rise, when the karstified relief was partially submerged [7].

In general, present-day coastal lakes and wetlands started to evolve in the last 120,000 years [6], when the mean global sea level was comparable to the present one [8]. About 20,000 years ago, during the LGM, the sea level was 120-m below the present mean sea level [8], causing the existence of coastal wetlands along those coasts that were not buried by permanent ice. Rapid and global sea-level rise from the LGM period made a high disturbance for coastal ecosystems. In the Holocene, the sea level rose from about 60 m to 1 m, and the mean sea level reached its present, world-averaged level about 6000 years ago [8,9]. Mediterranean coastal lowlands are affected by the Holocene marine transgression, which led to the flooding of closed basins and embayments [10–17].

The natural coastline of the Eastern Adriatic Sea was affected by changes in sea level during the Late Pleistocene and Holocene. Vast areas were dry land between the islands representing depressions and valleys, i.e., karst poljes, intersected by river flows [10–17]. Isolated karstic basins evolved from freshwater lakes and karst poljes to marine lakes during the last 50,000 years, as indicated by a sedimentary record in Lošinj Bay in the northern Adriatic Sea [15]. The coast retreated from an advancing sea, and the sea drowned the Late-Pleistocene/Early-Holocene landscapes. This is evidenced on the eastern Adriatic coast by submerged freshwater lakes and wetlands in Lake Veliko and Stupa Bay on the Island of Mljet [16,18], in Pirovac Bay [19], as well as a sub-marine archaeological Roman site and salt marsh in the Caska Bay on the Island of Pag [20,21], and prehistoric pile-dwellings in Zambratija Bay [22]. Most of the freshwater lakes on the eastern Adriatic coastal area formed during the Late Pleistocene/Early Holocene, such as Lake Vrana [23–25], a lake in Bokanjačko Blato [26], the Baćina Lakes (Crniševo) [19], and Lake Veliko on the Island of Mljet [16–18,27]. Holocene palaeohydrological changes from shallow to deeper lakes are driven by the sea level rise, while climate variability was only partly recorded, also due to the low resolution. Lake sediments from these lakes provide records of Holocene paleoenvironmental changes containing a combination of natural hydrological to climatic and anthropogenic signals, in relation to sea level rise and local catchment-specific processes. In the central and eastern Mediterranean, a wetter climate prevailed in early to mid-Holocene [28–31], followed by the drier climate conditions during the mid-Holocene, and several arid phases, with considerable site-to-site differences [2,31–33]. In the Adriatic Sea marine sediment core records, the wet early to mid-Holocene was determined [34,35], supported by the lake and marine sediment cores in the eastern Adriatic Sea [10,14,15,18,23,26,27,36,37]. High-resolution paleoclimate reconstruction was possible in lake sediments in the period of the deep-lake phase, between 8300 and 2600 cal yr BP, in Veliko Jezero on the Island of Mljet with four major and six minor cold and dry events identified [27], which correlates well with Adriatic marine cores [35,38].

Holocene climate conditions were reconstructed, with several wetter and dry periods during mid and early Holocene, using stable isotopes on speleothems from Croatian caves in Dalmatia, the Modrič Cave near the town of Zadar [39], Manita peć in the Velebit Mountains [40], Strašna peć on the Island of Dugi Otok [41], and two caves on the Island of Mljet [42]. All these mentioned lake, marine, and speleothem records from coastal Croatia are compared with the isotopic signal from speleothem data from continental Croatia, namely, from the Nova Grgosova Cave [43].

Holocene sea-level rise data points were determined on specific localities on the Eastern Adriatic Sea: in Lošinj Bay [14,15], in Novigrad and the Karin Sea [44,45], in Veliko Jezero and Stupa Bay on the Island of Mljet [16,27], in Caska Bay on the Island of Pag [20], in western Istria [46], in the Mirna and Neretva valleys [47], and on submerged speleothem records along the eastern Adriatic coast [48,49]. The salt pans and fish tanks were also used as sea-level markers on the eastern Adriatic coast [50–52], as well as archaeological and biological markers [53–55].

The coastal marine and estuarine environments along the eastern Adriatic coast were investigated using the marine and lake sediment cores at specific locations [14,56–66]. The studies of Dolenec et al. [67] and De Lazzari et al. [68] provided geochemical data for surface sediments along the southern part of the eastern Adriatic coast (EAC). The studies of trace elements in sediments of the central-southern Adriatic Sea indicate that contamination is only limited to specific areas [69]. Based on the analysis of a core from the MAD, trace element concentrations are consistent with the average composition of fine-grained middle Adriatic sediments, and major variations depend on changes in the silicate/carbonate ratios and the type and abundance of silicate supply [70]. The depth profiles of short marine sediment cores, collected at locations on a transect along the western rim of the EAC, showed that there is no contamination with priority contaminants in aquatic systems (As, Cd, Cr, Cu, Hg, Ni, Pb, and Zn). At the same time, Mo, Mn, Al, and Ca were identified as geogenic elements in those sediments, and the elemental composition was used to trace sediment sources [19]. Coastal lakes and wetlands host large and dynamic reservoirs of organic carbon. Higher values of TOC are evident in isolated karst basins during the freshwater phase, compared to recent marine and lake sediments [14,15,23,26,27].

In karstic areas, surface and underground water circulation are vital to the sedimentation processes, chemistry, and biology of coastal lakes and wetlands [6]. There is vital feedback between fresh and saline groundwater flows, sediment dynamics and organic matter mineralization, and the constantly changing geomorphology of coastal lakes and wetlands. Physical factors, such as water level, salinity range, and rising sea level, determine the type of coastal lake and wetland at a particular site. All the coastal lakes respond to sediment sources. Available material deposited in the basin influences the sedimentary environment. Sediment accumulation through deposition is a critical process because it maintains the relationship between a lake and wetland surface and sea-level change.

The evolution of coastal lakes and wetlands, Velo, Malo, and Kolanjsko Blato of the Pag Island on the central part of the eastern Adriatic coast (Figure 1) is examined using lake sediment cores. Paleoenvironmental reconstruction relied on the sedimentary records using grain-size, mineralogical and elemental composition, organic carbon and nitrogen content, and natural and anthropogenic radionuclides, coupled with micropaleontological ostracod analyses. The overall objective of this study is to identify paleolimnological and paleo-hydrological processes controlling the Holocene evolution of karst lakes in the coastal karstic region of Croatia using multiproxy methods. The Island of Pag, hosting the studied lake and wetlands, is a geologically highly complex low-lying karst coastal environment under the marine influence. As such, the karst lakes are well suited to be used to monitor environmental changes based on the interplay of sea-level rise and hydrological conditions due to changes in groundwater level and precipitation. Variations in lake levels during the Holocene were determined, which significantly influenced lake–wetland geochemical processes and vegetation habitats. Although the sea water intrusion is not the prime focus of the present paper, the process is considered most relevant, for the formation of these water bodies and the sediments play a crucial role as archives of the paleo-hydrological conditions. Records of multiple variables archived in sediment successions were used to evaluate environmental changes across time scales beyond the reach of monitoring data.

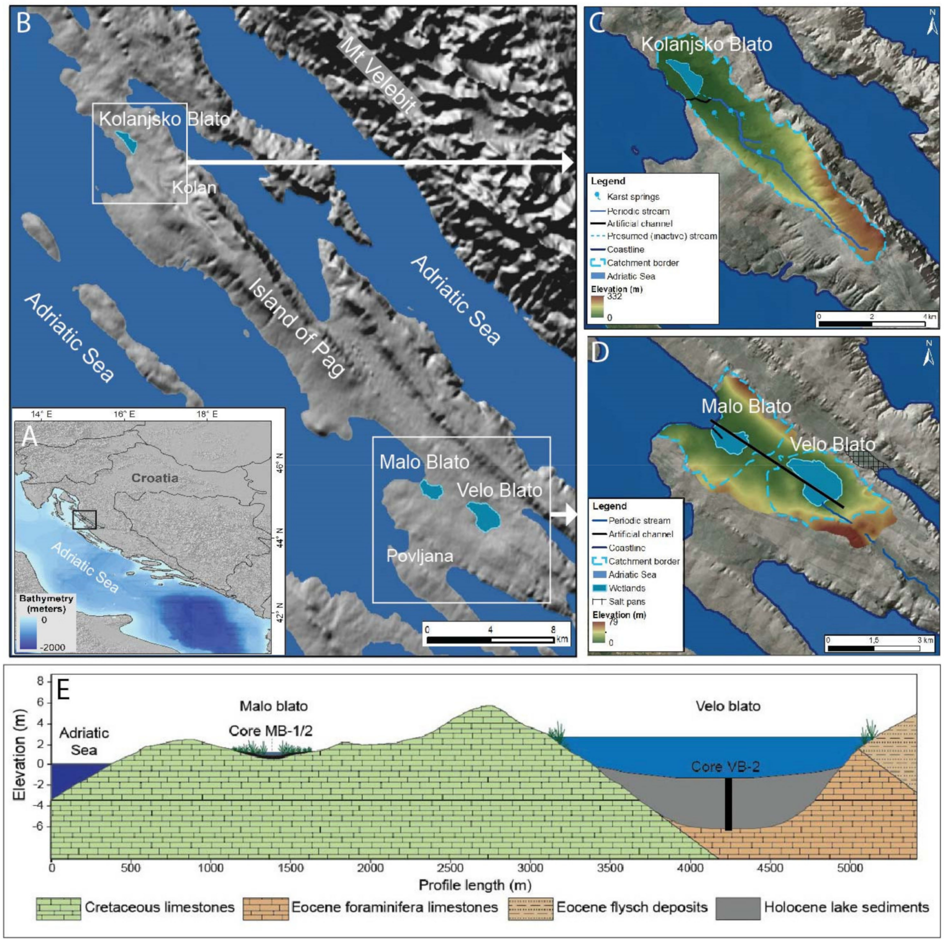

Figure 1. (**A**) The Island of Pag in Croatia, in the central part of the eastern Adriatic coast (black rectangle) (**B**) The study locations of Kolanjsko, Malo and Velo Blato on the Island of Pag; shallow coastal wetland Kolanjsko Blato (**C**) and lake Velo Blato and wetland Malo Blato (**D**) detailed maps with catchments area. The black line in figure D presents a profile through Velo and Malo Blato (**E**) to emphasize geomorphological and geological settings. Note that boundaries between geological units are schematic.

2. Materials and Methods

2.1. Study Site

Velo, Malo, and Kolanjsko Blato are coastal shallow lakes and wetlands in the central and southwestern part of the Island of Pag. The Island of Pag lies on the eastern Adriatic coast in Croatia, a typical Dalmatian-type coast with chains of islands and channels parallel to the coastline [71]. It is part of the Northern Dalmatian Archipelago, elongated in a NW–SE direction (Dinaric strike) in a length of approximately 60 km, and only 2 to 10 km wide. It is one of the largest islands on the Croatian coast (284.2 km^2), and the most indented, with a 302.5-km long shoreline [72]. The Island of Pag is characterized by low altitudes (the highest peak is 349 m asl.), with the most settlements located at an altitude of up to 50 m, except for a few settlements located at altitudes up to 100 m (Kolan and settlements on the Lun peninsula). Geologically, it belongs to the External Dinarides, which are a part of the Adriatic carbonate platform (AdCP) [73].

On the island of Pag, Upper Cretaceous rudist limestones predominate, followed by Upper Cretaceous limestones and dolomites and Paleogene clastic rocks (Eocene foraminiferal limestones and flysch) (Figure 2) [74–77]. On the Island of Pag there are occurrences of Eocene bauxite deposits. Miocene lacustrine deposits on Pag, presented by marls, clays, and sandstones with coal, are restricted to two NW–SE elongated basins, developed in two isolated syncline cores, Kolanjsko polje and the Crnika area [78,79], with most of the Miocene deposits hidden below the Pleistocene and Holocene sand and debris. The lacustrine sediments transgressively onlap the Cretaceous basement and attain a maximal thickness of 140 m in Kolanjsko polje [77]. Brown coal with black clay and lignite appears within lacustrine deposits in Kolanjsko Polje, and it was commercially exploited in the 19th and the first half of the 20th century. Quaternary sediments (alluvial/colluvial sands and clays) fill the larger dolines (karst valleys), such as Kolanjsko, Novaljsko, Paško, Dinjiško, Povljansko, and Vlašićko polje. Paško and Dinjiško polje are used as salt pans for salt production.

Figure 2. Geological map of the Island of Pag, with study locations Velo, Malo, and Kolanjsko Blato (modified after [74–77]).

Generally, relief is in accordance with the geological structure, which means the anticlines correspond to the highest parts of the island and the synclines correspond to shallow depressions. Valleys and poljes filled with Paleogene clastic rocks (Eocene marls, sandstones, and foraminiferal limestones), covered by Quaternary deposits (clay, sand) are favorable for water accumulation [80,81]. The anticlines, composed of Upper Cretaceous rudist limestones and dolomites, and Paleogene foraminiferal limestones, can direct groundwater flow locally, depending on the ratio of dolomitic layers in their cores. Infiltrated water naturally outflows on a large number of small coastal springs and vruljas, but in geologically and morphologically favorable zones, such as poljes, small local karst aquifers can be formed. Due to the relatively low altitude of that part of the terrain, a lake was formed on Velo Blato. That lake is in direct connection with a karst aquifer, and is slightly brackish; the chloride ion content is partially derived from the underground transition or mixing zone, and partially origins from the small seawater spray particles brought by strong NE wind bora. Although geological and morphological relations (high indentation and lack of favorably situated groundwater barriers) do not allow the formation of larger karst aquifers, the Island of Pag has several small aquifers, and some of them were used for public water supply. They are mutually not connected, and extracted quantities are limited. In the north-western shores of Lake Velo Blato, the pumping station was built for the public water supply in 1971. The groundwater and the slightly brackish surface lake water of Velo Blato was used mainly. In recent years, it has not been used frequently for water supply because of the limited water quality due to salinization problems [81,82]. The hydrogeological study confirmed that salinity increases with depth, with significantly higher values at approximately 15 m bsl [82]. The groundwater and surface water characteristics also vary according to the season, especially in chloride content and electrical conductivity, as well as in oxygen concentrations (Table 1). The data shown are derived from the water pumping station of Velo Blato between 2016 and 2018 (4 measurements annually), compared to the surface waters from Velo, Malo, and Kolanjsko Blato, which were measured within this study.

Table 1. Groundwater characteristics and geochemistry from the water pumping station of Velo Blato (VB), measured between 2016 and 2018, and presented as winter (November–May) and summer (July–October) periods; and surface water samples from Velo (VB), Malo (MB), and Kolanjsko (KB) Blato, measured in this study.

Water Sample	VB Water Pumping Station (Winter)	VB Water Pumping Station (Summer)	VB-1 (NW Part)	VB-2 (E Part)	MB-1	KB-1 (W Part)	KB-2 (Central Part)	KB-3 (E Part)
T (°C)	14.2	21.1	10.1	11.2	9	7.9	8.9	9.3
pH	7.4	7.7	8.32	8.5	7.8	8.11	8.18	8.26
O_2 (mg/L)	4.3	6.6	11.6	13.4	11	10.8	11.6	11.9
EC (mS/cm)	1.75	2.27	2.08	2.09	3.8	4.88	9.8	9.55
Cl^- (mg/L)	404.7	617.2	996.6	1000.1	1898.1	2700.8	6257.9	6042.3
NO_2^- (mg/L)	0.31	<0.009	<0.01	0.31	<0.01	<0.01	<0.01	<0.01
NO_3^- (mg/L)	0.45	0.45	0.37	0.39	0.7	<0.1	<0.1	<0.1
SO_4^{2-} (mg/L)	85.4	91.8	92.2	90.7	176.4	216.6	584.8	569.7
NH_4^+ (mg/L)	0.1	0.4	0.06	0.04	0.01	0.04	<0.01	<0.01
Ca^{2+} (mg/L)	n.a. *	n.a. *	82.5	82.1	108.1	114	145.1	138.1
Mg^{2+} (mg/L)	n.a. *	n.a. *	30.6	30.8	53.9	77.2	166.8	161.7
Na^+ (mg/L)	n.a. *	n.a. *	575.1	575.9	1118.6	1618.4	3604.7	3554.3
K^+ (mg/L)	n.a. *	n.a. *	9.1	9.2	17.0	23.9	57.9	56.2
HCO_3^- (mg/L)	n.a. *	n.a. *	250	250	280	360	380	370
TN (mg/L)	0.002	0.0024	n.a. *	n.a. *	n.a. *	n.a. *	n.a. *	n.a. *
TP (mg/L)	0.0058	0.0082	n.a. *	n.a. *	n.a. *	n.a. *	n.a. *	n.a. *

T—temperature; EC—electrical conductivity; * n.a.—not analyzed.

Coastal lake Velo Blato and wetland Malo Blato are located near Povljana, and they are approximately 1.5 km apart, with an up to 5-m high ridge between them. The total catchment area is 23 km^2. Velo Blato is the largest freshwater lake on the Island of Pag and represents an open-water surface area (surface 2 km^2). Nearby, Malo Blato (surface 0.9 km^2) comprises a larger wetland area that is rarely filled with water; only a smaller central part represents the permanent water body of Malo Blato. Malo Blato directly connects to the sea through the 450-m long artificial drainage canal, probably built before the 19th century. Velo Blato is located further away from the sea, without a direct connection to the sea. The large part of the lake is covered with wetland flora, especially reedbeds (reeds) and sedges, mainly in the north-western parts. Flora extends towards the central part of the lake in parallel lines perpendicular to the direction of the lake. The lake is a cryptodepression, with an average water depth between 0.5 and 2.36 m [83]. It has no inflow or outflow rivers, only periodic streams on the south-eastern shores of the lake that occur during wet seasons. The lake level in Velo Blato strongly depends on the precipitation and groundwater level [75,76]. It was noted that lake levels varied between 0.5 and 2.36 m asl. during the five years of monitoring within the hydrogeological research of its sanitary protection zones [82]. The seasonal variations in lake levels in Malo, Velo, and Kolanjsko Blato are visible in the false-color composite Sentinel-2 satellite images [84]. False-color composite is commonly used to study vegetation and its density (red color) and can be easily distinguished from the water and sea, which appear black or blue (Figure 3). Malo Blato is dominantly under the influence of daily tides, and the seasonal wet and dry periods have less impact on water level at Malo Blato than at Kolanjsko and Velo Blato, which have higher water levels in the wet period (Figure 3).

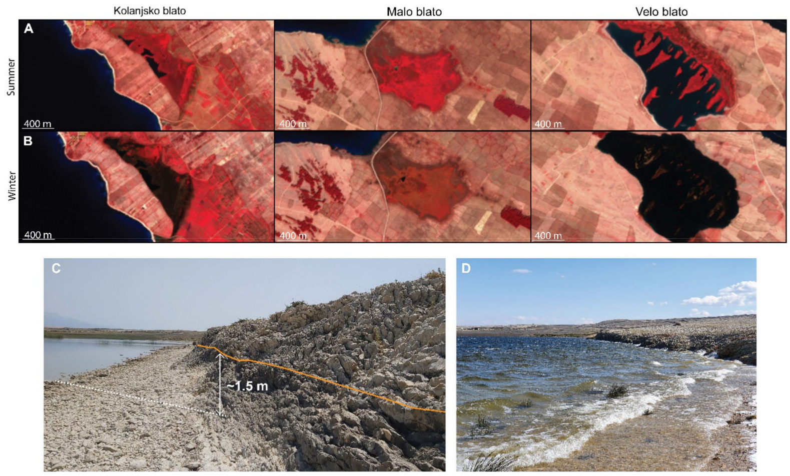

Figure 3. Satellite images (false-color composite Sentinel-2) of Kolanjsko, Malo, and Velo Blato during the dry (**A**) and wet (**B**) seasons in 2021 [84]; photos of the Lake Velo Blato surface level during the dry (June 2021; (**C**)) and wet (March 2021; (**D**)) periods—the lake level was up to 1.5-m lower during dry periods.

Kolanjsko Blato is located further away from Velo and Malo Blato, in the north-western direction, near Kolan. It comprises a larger water surface area during wet periods of the year in winter months, while, during summer months, the lake level decreases and three irregular shaped water bodies appear, separated from one another only by wetland vegetation (Figure 3). The catchment area is 23 km^2. It is separated from the sea through the carbonate ridge to the SE–S direction, 300- to 500-m wide. Geomorphological characteristics of the terrain indicate the surficial connection to the sea through the narrow artificial canal in the area of Rogoza, in the SW edge of the Kolanjsko Blato, through which the sea enters the Kolanjsko Blato at high tides; at low tides and at high water levels, the freshwater is drained into the sea. At the geomorphologically lowest part of the lagoon, salinity is occasionally higher. All together, they form a Kolanjsko Blato–Blato Rogoza lake–wetland ecosystem.

The climate of the Island of Pag belongs to a warm humid climate with hot summers—a Cfa type, according to Köppen's classification [85]. The average annual air temperature is 15.5 °C, and the average annual precipitation is 978 mm, with maximum precipitation between March and June (from 1981 to 2000, meteorological station Pag [86]). The whole island is exposed to the blows of the north-eastern wind bora; therefore, the vegetation is low and degraded, especially in very windy areas. The average number of days with strong or stormy winds was 23.5, while the mean number was 3.5 days, most of which occurred during winter (from December to March). During a period of strong bora winds, the sea salt is spread through the air throughout the island.

Velo, Malo, and Kolanjsko Blato represent freshwater-to-brackish wetlands, with characteristic wetland flora, fauna, and habitats. In vegetation, annual halophytes (Salicornia in Velo and Malo Blato, Cakiletea maritimae p. in Kolanjsko Blato) predominate. Salicornia is a salt-tolerant halophyte flowering plant that usually grows in salt marshes. Other species in the area of Malo Blato include *Cladium mariscus*, which was rare in the past, but its number has increased during the past 80 years [86]. It usually grows on peat at the margins of the lakes and ponds. Habitats that prevail in Velo and Malo Blato are Mediterranean sitine (*Juncetalia maritimi*), Mediterranean and thermoatlantic vegetation of halophilous shrubs (*Sarcocornetea fruticosi*), Isoeto-Nanojuncetea wetland habitats, eastern sub-Mediterranean dry grasslands, and natural eutrophic waters with Hydrocharition or Magnopotamion vegetation. The habitats of Kolanjsko Blato belong to coastal lagoons, eastern sub-Mediterranean dry grasslands, Mediterranean occasional pools, Mediterranean sitine, sub-Mediterranean wet grasslands, Molinio–Horedion. In Velo and Malo Blato appear wetland birds, spindles, and butterflies. Various birds, such as herons, gleaming ibis, and especially turkeys, the great reed warbler and the silkworm, various species of woodpeckers, and many others inhabit Kolanjsko Blato. The endangered sea sandpiper, a nesting bird of Pag salt pans, appears here, in addition to spindles, land and pond turtles, red snakes, meadow clefts, and butterflies. In the past, there has been evidence of the presence of eels in Lake Velo Blato [83]. Grazing sheep maintain the surrounding dry pastures. Both Velo and Malo Blato, as well as Kolanjsko Blato, are protected areas as Ornithological Reserves since 1988, and are managed by the Public Institution Natura Jadera, Zadar County. These reserves are part of ecological networks HR4000004 and HR2000911.

2.2. Sampling and Side-Scan Sonar Survey

A long sediment core in Velo Blato (VB-2, 0–568 cm) was extracted from the central part (44°21.292′ N, 15°9.308′ E) at the water depth of 2.7 m (Figure 4) using the Uwitec piston corer, which consists of rope-operated piston corer mounted on a tripod tower on an aluminum platform and pontoon floaters. The coring is performed by a hammer from the platform, using 3-m long plastic liners, 60 mm in diameter, in a stainless steel liner, and it is possible to retrieve contiguous 3-m sections of the sediment core. Due to the limited access and unapproachable terrain of the water bodies of Kolanjsko and Malo Blato, the sediment sampling was made possible only by rubber boats (in the case of Kolanjsko Blato) or by foot (in the case of Malo Blato) (both in March 2020). As a result, the sediment cores recovered from these lakes are only 107-cm long from Kolanjsko Blato (KB-1; 44°31.442′ N, 14°54.662′ E) and 35-cm long from Malo Blato (MB-1/2; 44°22.017′ N, 15°7.114′ E) (Figure 5). The sampling campaign was performed in April 2020. The cores were transported into the laboratory of the Croatian Geological Survey for core description and sub-sampling. The cores were split lengthwise and photographed. Archive halves were stored in the cooling chamber. In addition, several short sediment cores (<50 cm) and grab samples were collected in Velo Blato using a gravity corer and a Van Veen grab sampler, respectively (Uwitec, Mondsee, Austria). On the southern shores of Lake Velo Blato, the samples of flysch marls were taken for mineralogical analysis.

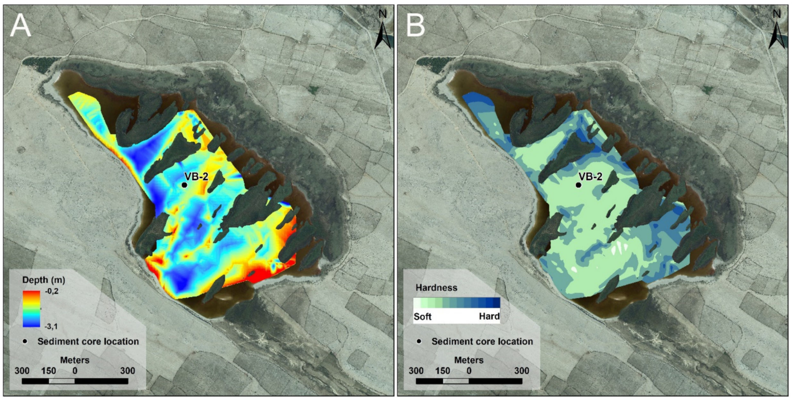

Figure 4. Lake Velo Blato images obtained using side-scan sonar: (**A**) lake bathymetry map; (**B**) back-scatter images (sediment "hardness") map. Sediment core location VB-2 is marked on both maps.

Figure 5. Sampling locations in Kolanjsko (**A**) and Malo Blato (**B**).

During fieldwork in March 2020, the surface water was sampled in Velo Blato—2 locations, Kolanjsko Blato—3 locations, and Malo Blato—1 location. Prior to sampling, the field parameters of electrical conductivity (EC), temperature (T), pH, and dissolved oxygen (DO) were measured using a portable multiparameter probe (WTW). Basic anions and cations were determined using the ion chromatograph Dionex ICS 6000 in the Hydrochemical Laboratory of the Croatian Geological Survey. The results are compared to groundwater from water pumping station Velo Blato and presented in Table 1.

Side-scan sonar (SSS) was used to better understand the morphology and bathymetry of the lakebed. The survey was conducted in Lake Velo Blato (Figure 4). A side-scan sonar Humminbird 999 HD SI was used, which was mounted on a small rubber boat. This side-scan sonar device operates at frequencies of 80 or 200 kHz with an external Humminbird AS + GPS HS antenna and heading sensor used for positioning.

2.3. Sedimentological and Mineralogical Analysis

The sediment cores from Velo and Kolanjsko Blato were imaged, and spectral color measurements were performed, using an X-Rite spectrophotometer (DTP22). Magnetic susceptibility was measured (MS, SI units $\times 10^{-5}$) using a Bartington MS2E surface sensor with a 1-cm resolution. In addition, wet/dry bulk density and water percentage were measured in 70 samples throughout the sediment core from Velo Blato. Smear slides were prepared using Norland 61 optical adhesive and a UV lamp on glass slides. Grain-size analysis was performed using a Shimadzu SALD-2300 laser diffractometer, between 0.17-µm and 2-mm particle size. Samples (0.2 g) were pre-treated with 30% H_2O_2 on a hot plate at 80 °C to remove the organic matter. Next, 2 mL ($Na_4P_2O_7$) was added as a dispersant; then, the samples were sonicated before being analyzed. The obtained result for every sample is the average of three measurements. The data were processed using the software GRADISTAT v8 [87]. In total, thirty-seven samples were measured for grain-size from a sediment core from Velo Blato, and ten samples were measured from both Malo and Kolanjsko Blato. Mineralogy was determined on selected samples by a PANalytical X'Pert Powder X-ray diffractometer (Cu Kα, 45 kV, 40 mA, Ni filter). The back-loading technique was used for specimen preparation of the powdered samples. The angular range of measurements was 4° to 66°2θ. Identification was performed using HighScore X'Pert Plus software by ICDD database (PDF-4/Minerals) and XRD patterns [88]. The bulk mineralogical composition was determined for thirty-eight samples from Velo, Malo, and Kolanjsko Blato. The clay mineral analysis on oriented samples was performed on two samples from the sediment core from Velo Blato (289–296 cm, 445–446 cm) and flysch marls from the southern lake shores of Velo Blato. The clay fraction was prepared after calcite removal on glass slides, and the clay minerals were identified after air drying, ethylene glycol saturation, and heating to 400 and 550 °C [88].

2.4. Geochemical Analysis

Geochemical analyses were performed as quantitative elemental assays of forty-five major and trace elements, in addition to Hg, on 52 samples covering all sedimentary facies, by Inductively Coupled Plasma-Mass Spectrometry (ICP-MS) and Inductively Coupled Plasma-Emission Spectrometry (ICP-MS and ICP-ES), at the commercial laboratory Bureau Veritas in Vancouver, Canada. Samples (1 g) were dissolved in multi-acid (HCl-HNO_3-$HClO_4$-HF) at 200 °C. Mercury (Hg) was dissolved using aqua regia digestion. Reference standard materials were STD DS11, STD OREAS262, STD BVGEO01, STD OREAS25A-4A, and STD OREAS45H.

The Enrichment Factors (EF) of selected elements were used to estimate the status of environmental contamination and the degree of anthropogenic heavy metal pollution. Element concentrations are normalized against an immobile conservative element to eliminate grain-size effects and dilution by mineral phases such as quartz and carbonates. Al is the most frequently used geochemical normalizer in coastal and marine sediments, based on the assumption that Al is present in terrigenous (detrital) aluminosilicates [89–91]. Background reference values were taken from deeper layers [92]. Trace metals that derive entirely from naturally occurring rocks and weathering processes display values between 0.5–1.5, whereas trace metals from dominantly anthropogenic sources show values greater than 1.5 [93]. The EF values were calculated using Formula (1) given in Zhang et al. [93]:

$$\mathrm{Ef} = (\mathrm{Metal}/\mathrm{Al})\mathrm{sample}/(\mathrm{Metal}/\mathrm{Al})\mathrm{background} \quad (1)$$

The sediment core from Velo Blato was sub-sampled every 5 cm in the upper part of the core (0–200 cm) and every 10 to 15 cm in the lower part of the core (200–550 cm) for Total Carbon (TC) and Total Nitrogen (TN), and Total Organic (TOC) and Total Inorganic (TIC) Carbon. In total, seventy-one samples from the Velo Blato sediment core, and ten samples from both Malo and Kolanjsko Blato, were analyzed. They were measured with a CN elemental analyzer, Thermo Fisher Flash2000. Total carbon (TC) and nitrogen (TN) were measured directly, while total organic carbon (TOC) was measured after the removal of carbonates using 4M HCl and heating for 2 h. Total inorganic carbon (TIC) was calculated as the difference between TC and TOC. The C/N ratio was calculated by dividing the TOC and TN.

2.5. Ostracod Analysis

For micropaleontological analyses, forty-three samples were taken from the Velo Blato sediment core (VB-2), and ten samples from both Malo (MB-1/2) and Kolanjsko (KB-1/1) Blato. The sampling resolution was, in general, 1 cm, but it sometimes needed to be 2 or 4 cm (for the topmost sample) due to high organic matter contents in the sediments. The samples were first freeze-dried, after which they weighed at ~5 g (Malo and Velo Blato) and ~3 g (Kolanjsko Blato). The freeze-drying method was shown to be very successful in preparing micropaleontological samples from lake sediments. Thus, no additional chemical treatment was used during the preparation. The samples were wet-sieved with distilled water to 400 and 125 µm, and finally, they were oven-dried at 40 °C. Samples from all sediment cores (Malo, Velo, and Kolanjsko Blato) were examined qualitatively to determine the general species variability and general fossil content in the recent sediments from all wetlands. Preliminary qualitative analyses of the samples from the VB-2 sediment core from Velo Blato showed greater potential for the quantitative ostracod analysis. Samples from Velo Blato are very rich in ostracods, and they contained some smaller species which were not present in the 400-µm fraction (e.g., *Limnocythere inopinata* and *Cypria ophtalmica*). Thus, it was decided to re-sift previous and additional samples to 0.2 and 0.125 µm, and only the larger size fraction was quantitatively analyzed. The dry-sieved sediment was weighed, and samples were analyzed using the AmScope 3.5×–90× trinocular zoom stereomicroscope. Due to the high abundances of the species, ostracod shells were manually picked only from the 0.2-mm fraction using a fine brush and deionized water. Abundances were normalized to 1 g of dry sieved sediment. Species identification was based on Fuhrman [94] and Meisch [95].

2.6. Radioactivity Measurements

The gamma-spectrometry was performed on short sediment cores from Velo and Kolanjsko Blato. Cores were sliced in 1-cm intervals, dried in a freeze-dryer, and ground to ensure homogeneity. Samples were packed in 100-cm^3 volume geometry, sealed, and left for four weeks to establish radiochemical equilibrium before the activities of radionuclides (^{214}Bi, ^{137}Cs, ^{40}K, ^{210}Pb and ^{226}Ra) were determined. The sample masses varied from 9.5 to 26.6 g. The radioactivity measurements were performed on 20 samples (10 per sediment core from Velo and Kolanjsko Blato) at the Institute for Medical Research and Occupational Health in Zagreb, using ORTEC p-type coaxial high purity germanium (HPGe) detectors. The data acquisition was performed using a computerized system (GammaVision software). Samples were counted for a minimum of 80.000 s. Activity concentrations of ^{137}Cs were used to determine the sedimentation rate on the analyzed sediment cores. The calibration of the measurement setup was carried out using standards prepared by the Czech Metrology Institute, whereas quality assurance was performed through regular participation in interlaboratory comparisons organized by the International Atomic Energy Agency (IAEA), World Health Organization (WHO), and European Union Joint Research Centre (JRC).

2.7. Radiocarbon Dating

Throughout the Velo Blato sediment core, a total of seven samples were selected for accelerator mass spectrometry (AMS ^{14}C) measurements, of which five were shells (freshwater/terrestrial). Two samples were plant materials from the same depths as shells (at 105–106 cm and 308–309 cm) to determine the reservoir hardwater effect due to the carbonate watershed. In Kolanjsko Blato, three samples of shells (marine) were used to obtain the radiocarbon age. The radiocarbon dating was carried out at the Beta Analytics Laboratory, Miami, USA. The Conventional Radiocarbon Age (BP), Percent Modern Carbon (pMC), and stable isotopes (δ^{13}C and δ^{18}O) were provided. The age is reported as radiocarbon years before present (BP; "present" = AD 1950). Radiocarbon dates were calibrated using the INTCAL20 database [96] for freshwater samples from Velo Blato, and MARINE20 [97] for marine samples from Kolanjsko Blato. The 95.4% distribution (2σ probability interval) was taken into account to build the age–depth model using CLAM 2.2 software.

3. Results

3.1. Sedimentological and Mineralogical Description of Sediment Cores

Along the sediment core from Velo Blato (0–557 cm, +11 cm in core catcher), changes in the color of the sediment are visible from dark grey, almost black in the upper 21 cm, to the bright lake carbonate sediment with occasional layers of darker sediment. Darker layers have an evident decrease in the brightness color value L* (Figure 6). Shells and their fragments appear along the entire length of the sediment core, and certain intervals contain significantly accumulated shells, predominantly the shells of freshwater snail *Bithynia tentaculata*, especially between 130 and 300 cm (intervals: 137–140, 159–160, 219–221, 276–278, and 282–288 cm). In the lower parts of the core, they appear less frequently. From 300 to 557 cm, the sediment core is a brighter grey, less yellow and more bluish in color, with occasional dark intervals, especially from 439 to 450 cm and from 530 to 557 cm. The base of the drilled core (from 554 cm to 568 cm) is composed of limestone fragments as part of the weathered geological bedrock, i.e., flysch deposits. The lower parts of the core (from 530 to 550 cm), contain calcite predominantly, while between 504 and 445 cm, calcite and quartz are present in equal amounts; dolomite is also present, along with feldspar, muscovite/illite, kaolinite, pyrite, and aragonite. Clay minerals analysis showed the presence of the smectite, illite, and kaolinite, which presents the same clay mineral assemblage as the flysch marls from the southern shores of Velo Blato. From 388 to 102 cm, calcite with a significant proportion of magnesium is present, and can be defined as Mg-calcite. In the interval from 255 to 102 cm, magnesium calcite appears in the samples, along with quartz, aragonite, muscovite/illite, and halite. Low-Mg calcite is dominant in samples from 74 to 40 cm, with the appearance of quartz and aragonite as accessory phases. Equal amounts of calcite and quartz are present in samples from 25 to 0 cm, with muscovite/illite, aragonite, and pyrite. Halite is present in the samples as a result of sample drying. Aragonite is of biogenic origin, the result of the shell fragments grinding. Smear slide analysis of several surface sediment samples (VB-2 0–1, 10–11 cm) showed calcite and quartz grains in the lake sediment of Velo Blato, and a significant amount of algal organic matter was observed. Throughout the core, sponge spicules, diatoms, and ferrous sulfide mineral pyrite in the form of framboidal aggregates, composed of crystalline forms of hexahedra, occasionally appeared. The upper parts of the core have relatively lower dry densities and higher water contents, compared to the rest of the core (Figure 6). Magnetic susceptibility (MS) values are relatively low throughout the Velo Blato sediment core, especially in the upper parts of the core (from 60 cm and upward), where its values are negative on average (-0.52×10^{-5} SI) (Figure 6). The highest magnetic susceptibility values are between 438 and 450 cm, with the highest values of 4.7×10^{-5} SI. After this interval, the lower parts of the core show slightly higher values of magnetic susceptibility than the rest of the core (average 1.26×10^{-5} SI).

The sediments from the Kolanjsko Blato sediment core (KB-1/1), along its entire length of 107 cm, consist of a relatively homogeneous dark grey to black sediment, with occasional appearances of shell fragments. In the lower part of the core, at 95 cm until 107 cm, the sediment is full of fragments of shells (snails and marine shells). From 60 cm towards the deeper parts, the sediment becomes light grey in color. In the upper part of the core (from 60 cm upwards), the sediment contains plant remains and significant amounts of organic matter, which almost presents peat sediment. Within the sediment, larger pieces of coal were observed (>0.5 cm), which are probably derived from the Kolanjsko Polje from Miocene deposits that contain coal and lignite, which was exploited in the last century, having been brought to the Kolanjsko Blato by surface streams. Therefore, although ideal for radiocarbon dating, this material is not used. In general, XRD analyses of sediment samples from Kolanjsko Blato have high background values and low diffraction maximum (peaks). Such diffractograms indicate significant amounts of organic matter in the samples. In the lower parts of the core (105–60 cm), sediment samples contain calcite, quartz, aragonite, pyrite, halite, muscovite/illite, and in the lowest sample (105–106 cm), also kaolinite and clay minerals (Sm/Verm/Chl). From 50 to 0 cm, calcite, Mg-calcite, aragonite, quartz, pyrite, halite, and muscovite/illite are present in the samples. In the uppermost sample (0–2 cm), Mg-calcite was not observed.

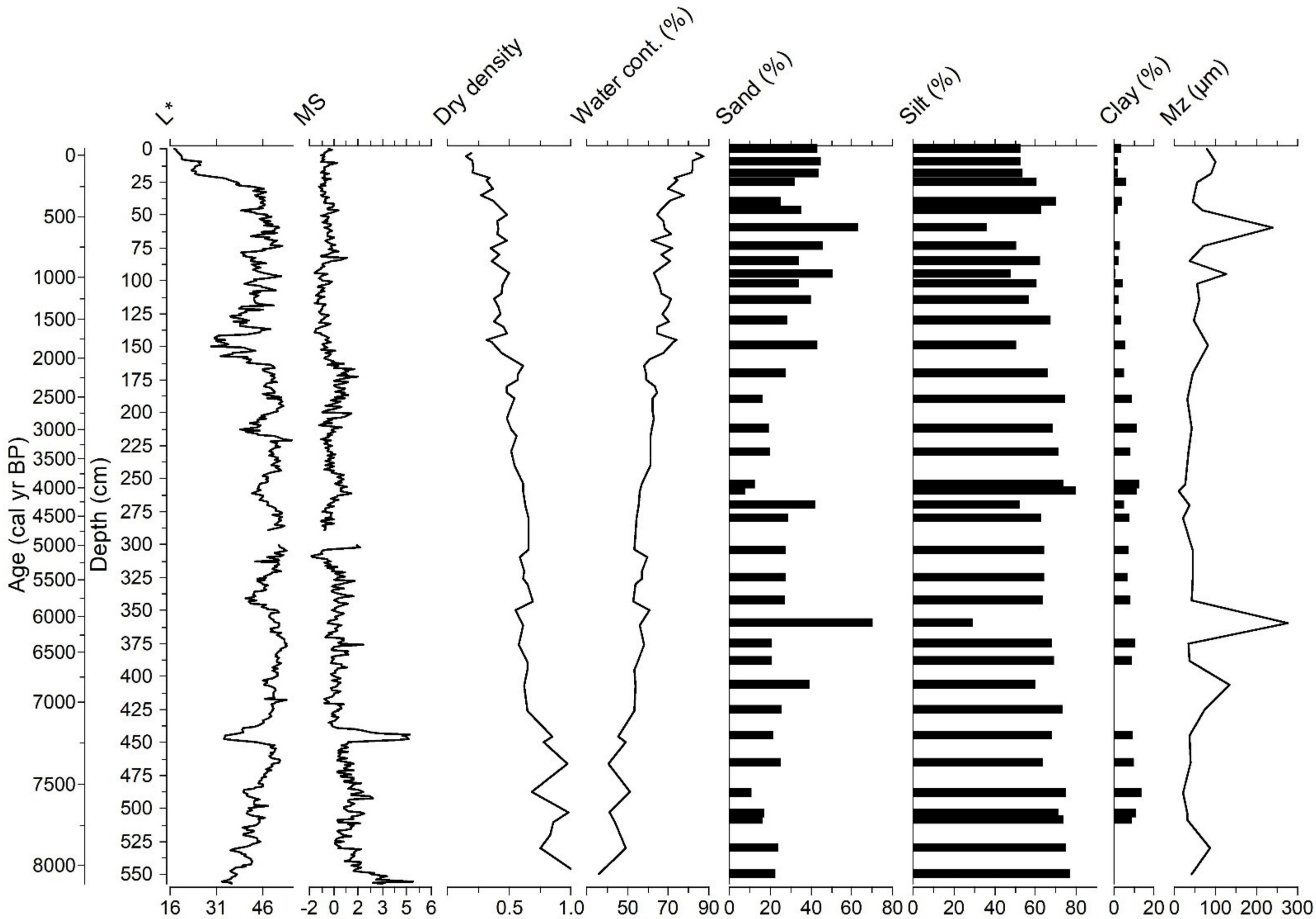

Figure 6. Color brightness (L*), magnetic susceptibility (MS; 10^{-5} SI), dry density (g/cm^3), water content, and grain-size down-core variation in the sediment core VB-2 from Lake Velo Blato.

Samples from the sediment core from Malo Blato contain, in the lower parts of the core (34–24 cm), predominantly quartz and calcite, muscovite/illite, kaolinite, pyrite, aragonite, and clay minerals (Sm/Verm/Chl) appear as minor mineral phases. From 20 to 0 cm, calcite and quartz are present in equal amounts in the samples, while aragonite and halite are minor minerals. As well as in sediments from Velo Blato, halite is present in the samples from Kolanjsko and Malo Blato as a result of sample drying, while aragonite derives from the grinding of the shell fragments.

3.2. Sediment Chronology

The chronology of the sediment core from Velo Blato is constrained by five radiocarbon dates obtained from freshwater shells (Table 2). To determine the reservoir effect, two additional samples from the same depths, at 105–106 cm and 308–309 cm, were measured for radiocarbon dating using plants. The reservoir effect in the interval of 105–106 cm is 80 years, while at a depth of 308–309 cm, it is 190 years, which are determined using shells and plants combined from the same intervals, but it should be emphasized that the reservoir effect could be higher because the plants can also uptake the old carbon from the water. The deepest analyzed sample in Velo Blato (552–554 cm) showed the age of the sediments deposited in Lake Velo Blato, and it is dated to the last 8300 years. In Kolanjsko Blato, the sample at the very bottom of the drilled core (106–107 cm) showed the age between 1100 and 2491 cal year BP. Two additional marine shell samples were used to constrain the depth–age model for the Kolanjsko Blato sediment core (Figure 7). The determined reservoir ages were calculated into the model for the depth–age model in Velo Blato (Figure 7).

Table 2. Radiocarbon dates obtained in the Velo (VB-2) and Kolanjsko Blato (KB-1/1) sediment cores.

Lab ID	Sample (cm)	Material	$\delta^{13}C$ (‰)	$\delta^{18}O$ (‰)	pMC	Conventional ^{14}C Age	Calendar Age (2σ Calibration)
Beta-591017	KB-1/1 55–56	Shell (marine)	−5.7	+1.5	95.26 ± 0.36	390 ± 30 BP	560-Post BP cal BP
Beta-591018	KB-1/1 77–78	Shell (marine)	−5.3	+0.3	85.27 ± 0.32	1280 ± 30 BP	1468–316 cal BP
Beta-591019	KB-1/1 106–107	Shell (marine)	−9.7	−0.2	76.80 ± 0.29	2120 ± 30 BP	2491–1110 cal BP
Beta-591020	VB-2 105–106	Shell (freshwater)	−3.1	−0.2	85.7 ± 0.32	1240 ± 30 BP	1192–1070 cal BP
Beta-591021	VB-2 105–106	Plant	−25.8		86.55 ± 0.32	1160 ± 30 BP	1130–972 cal BP
Beta-591022	VB-2 201–202	Shell (freshwater)	+0.1	−1.5	71.54 ± 0.27	2690 ± 30 BP	2851–2752 cal BP
Beta-591023	VB-2 308–309	Shell (freshwater)	−1.2	−2.2	55.71 ± 0.21	4700 ± 30 BP	5423–5321 cal BP
Beta-591024	VB-2 308–309	Plant	−25.8		57.04 ± 0.21	4510 ± 30 BP	5202–5048 cal BP
Beta-591025	VB-2 402–403	Shell (freshwater)	+2.9	−2.0	46.10 ± 0.17	6220 ± 30 BP	7134–7003 cal BP
Beta-591026	VB-2 552–554	Shell (freshwater)	−5.8	−1.9	39.56 ± 0.15	7450 ± 30 BP	8346–8187 cal BP

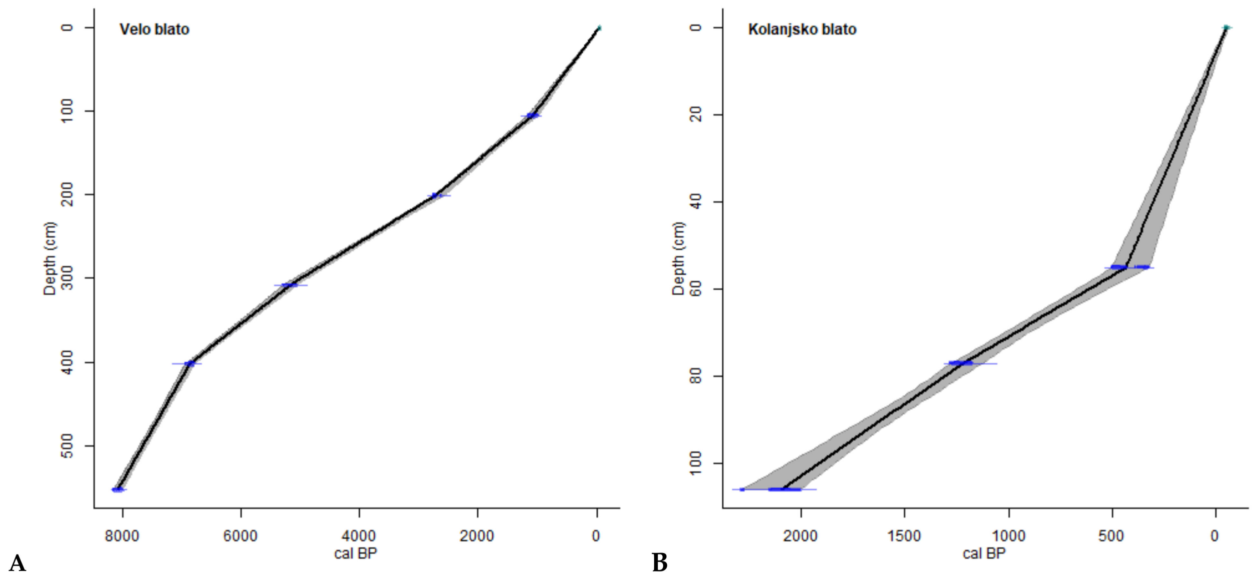

Figure 7. Depth–age models of sediment cores from (**A**) Lake Velo Blato (VB-2) and (**B**) Kolanjsko Blato (KB-1/1).

The sedimentation rate (SR) in Velo Blato is relatively high (1.24 mm/year) at the base of the core (554–402 cm), followed by slower SR in the middle part of the core (402–201 cm), where it varies between 0.4 and 0.6 mm/year. Again, the upper part of the core shows higher SR (0.9 mm/year). The sedimentation rate in Kolanjsko Blato is higher (1.1 mm/year) in the upper part of the core (0–55 cm), compared to the lower values (0.3 mm/year) in the lower part of the core (55–106 cm).

3.3. Grain-Size Analysis

Sediments from Velo Blato are predominantly silt-sized (63.2%), with a significant proportion of sand (30.9%), while the percentage of clay is ~5% (Figure 6). In the sand fraction, very fine sand prevails on average (17.3%) in relation to fine sand (7.5%), medium sand (4.9%), and coarse sand (1.2%). The most common silt fraction is very coarse silt (19.2%), followed by coarse silt (14.4%) and medium silt (13.3%). Fine silt and very fine silt are present in proportions less than 10%, except in the samples at 406–407 and 425–426 cm, which have higher proportions of medium silt (35.9 and 37.1%) and fine silt (17.2 and 16.0%) but do not contain a very fine silt fraction. These samples (406–407 and 425–426 cm) do not contain a clay fraction and are classified as coarse silts [98], as are the samples at 60–61 cm and 360–361 cm (very fine and fine sands), and the lower core samples at 530–531 and 550–551 cm (very coarse and coarse silts). In the sediment core, a higher proportion of sand (39.6%) is observed in the upper parts of the core (170–0 cm) than in the lower parts of the core (550–190 cm; 25.0%). At the same time, the silt and clay fractions are higher in the lower parts of the core (550–190 cm; 67.5% and 7.5%, respectively) compared to the upper part of the core (170–0 cm; 57.0% and 3.4%). The average clay content in the upper parts of the core (0–170 cm) is 3.4%, and in the lower parts (190–550 cm), 7.4%. More than 10% of the clay fraction have samples in the lower parts of the core, at 212–213 cm (12.0%) and 255–256 cm (13.1%), 375–376 cm (10.7%), and the interval between 465 and 504 cm (10.2–13.8%). The mean particle size (Mz) in the analyzed sediment samples is 33.5 µm, while in the sand samples, it is much higher than the average values (70.7–147.1) (Figure 6). Additionally, in these samples, the median particle size (Md) is much higher (63.5–289.5 µm) than the average values of the sediment core (40.7 µm). Bimodal and trimodal distributions of particle-size curves predominate in most samples, unimodal distribution is present in two samples (40–41 cm and 74–75 cm), while polymodal distribution is present in samples 25–26, 212–213 and 375–376 cm. All analyzed samples are very poorly to poorly sorted. According to asymmetry (skewness), the samples are mostly very positive and positive skewed (very fine, fine skewed), are partially symmetrical, and several samples show very negative and negative skew (very coarse, coarse skewed). According to the sharpness (kurtosis), the samples in the upper parts of the sediment core mostly have medium-pointed curves (mesokurtic), with occasional leptokurtic curves, while in the lower parts, the curves are platykurtic.

Sediment samples from Kolanjsko Blato consist of a significant amount of sand (44.0%) and silt (49.5%), while a clay fraction is present in only 6.5%. The sample at 30–31 cm is the only sample that contains a fraction of coarse sand (14.2%) and the highest amount of medium sand (38.4%), compared to the rest of the sediment samples, and does not contain clay fractions. In the sand fraction in the analyzed samples, very fine sand (21.6%) predominates, while in the silt fraction, very coarse silt predominates (17.1%). The individual particle-size curves of the analyzed sediment samples from Kolanjsko Blato show a mostly trimodal distribution, while the 0–1-, 10–11- and 50–51-cm samples have a bimodal distribution. Most of the samples are classified as very coarse and coarse silts, while the sample at 30–31 cm is classified as fine sand [98]. The samples are very poorly and poorly sorted, very positively and positively skewed, and primarily have medium-sharpened curves (mesokurtic), while the rest are platykurtic and/or leptokurtic. The average particle size (Mz) in the analyzed sediment samples is 32.1 µm, except in the sample of 30–31 cm, which is significantly higher (161.7 µm). Moreover, the median particle size (Md) is larger (268.9 µm) than the other samples (45.4 µm).

Sediment samples from Malo Blato consist mainly of a fraction of sand (55.8%) and silt (42.2%), with a clay fraction <2%. It is characteristic of the sample at 16–17 cm, which is predominantly sandy (95.6%) with a very low silt content (4.4%) and no clay present. Clay is also absent in other samples throughout the sediment core, and it is the highest in the lower sample, the interval at 30–31 cm (8.4%). In the sand fraction, the very fine sand (18.9%) is the most common, except in the sample at 16–17 cm, where coarse sand predominates (58.6%). The very coarse silt (17.0%) is the dominant silt fraction in all the samples. The particle-size distribution curve is mostly unimodal, and in some samples bimodal (30–31 cm), trimodal (4–5, 12–13 and 24–25 cm), and polymodal (34–35 cm). Most of the samples are classified as very coarse silts or very fine and fine sands [98]. The samples are generally poorly sorted, while in the lower parts of the core, the samples are very poorly sorted, and the sample at 16–17 cm is moderately well sorted. The kurtosis of the curves also varies from very platykurtic (34–35 cm), platykurtic (12–13 and 24–25 cm), mesokurtic (0–1, 4–5, 30–31 cm), leptokurtic (8–9, 10–11, 20–21 cm), to very leptokurtic (16–17 cm), and are generally very fine and fine skewed. The mean particle size (Mz) in the analyzed sediment samples is 120.6 µm, with the sample at 16–17 cm exceeding this value, with a Mz of 551.2 µm. In addition, this sample's median particle size (Md) is 604.0 µm, while the median of all samples is 147.4 µm.

3.4. Major and Trace Element Abundances

Elemental concentrations in the analyzed samples from the Velo Blato sediment core are presented by depth and age (Figure 8), and by descriptive statistics (Table 3). Concentrations of main lithogenic elements Al, Ti, Fe, K, and Na have similar vertical distributions, i.e., they are elevated in the samples in the lower parts of the core (550–445 cm), are relatively lower in the middle part of the core (425–47 cm), and increase in the upper part of the core (47–0 cm). The Al, Ti, Na, K, and Fe contents are the highest in the sample at 445–446 cm, in which the Ca content is much lower than the rest of the core. In addition to this interval, the Ca content is evenly distributed throughout the sediment core; the highest values appear in the interval of 95–47 cm, but from 47 cm of the core, it significantly decreases upward. The Mg content shows a different distribution than Ca and is different from Al and other siliciclastic elements. It is low in the base of the core, where it shows elevated concentrations in the interval between 509 and 445 cm, where dolomite appears in the sediments. The Sr concentration is lower from the base of the core to 425 cm, when it starts to have an increased trend upward, and the highest values are in the same interval where the Ca content is the highest. Sr and Ca have similar vertical trends and represent carbonate components, showing an elevation in the base of the core and a decrease in the upper part of the core from 47 cm upward. P and N content also show the same increase in the sediment core, from 47 to 0 cm. Other trace elements (As, Ba, Cd, Co, Cr, Cu, La, Ni, Pb, Rb, V, Zn, and Zr) show the same trend as the main lithogenic elements and are connected with the siliciclastic component. They have elevated concentrations in the lower and the upper part of the sediment core. Mn has elevated concentrations in the upper part of the core (47–20 cm), while the top of the sediment core decreases. At the same time, in the topmost samples, the content of Mo increases. The Hg concentrations are elevated in the lower part of the core, in the sample at 488–489 cm, and in the interval from 445 to 325 cm. Then, the proportion decreases and is very low, i.e., below the limit of detection in the interval of 130 to 60 cm, and then increases towards the top of the core, and is high in the surface sample (1–2 cm).

In the sediments from Kolanjsko Blato, the composition of the main elements, Al, Ti, and K, is elevated in the lower part of the core (from 105 to 60 cm) and decreases towards the upper parts of the core (Figure 9; Table 3). The share of Fe has a similar distribution, but it is quite low in the lowest sample (105–106 cm). The content of Na differs from the above elements—it is lowest in the lower part of the core, increases towards the upper parts of the core, and is highest in the sample at 1–2 cm. Mg and Sr concentrations have a similar trend to Na, which increases from the lower parts of the core upwards. On the other hand, the distribution of Ca with depth is similar to the distribution of lithogenic elements Al and Ti, i.e., it decreases from the base of the core upwards, and is lowest in the upper parts of the core. The shares of P and S increase from the bottom up, i.e., inversely from Al and Ti, and similarly to Na and Mg. The concentrations of trace elements Ba, Cr, La, Ni, Rb, V, and Zr in Kolanjsko Blato have a similar distribution as the main lithogenic elements: higher in the base of the core and decreasing upwards. The elements As, Cd, Co, Cu, Pb, Sr, and Zn deviate from this trend. The proportion of As is higher in the lower parts of the core

(105–60 cm) and lower in the upper parts of the core (40–0 cm). The Cd and Co contents are only higher in the samples at 90–91, 70–71, and 60–61 cm. The Pb concentrations are low in the lower parts of the core (105–106 cm, 90–91 cm), increases from 70 cm, and are relatively constant upwards, showing a slight increase in the surface sample (1–2 cm). The Zn content is also low in the lower part of the core and increases upwards, with a decrease in the sample at 10–11 cm. The concentrations of Cu are higher only in the surface sample (1–2 cm), as well as those of Mo. In the lower parts of the core, the Hg content is elevated in the sample at 90–91 cm, while it is low in the samples at 105–106 and 70–71 cm. The concentrations increase from the sample at 60–61 and are constant in the core's upper parts (50–10 cm), slightly increasing in the surface sample (1–2 cm).

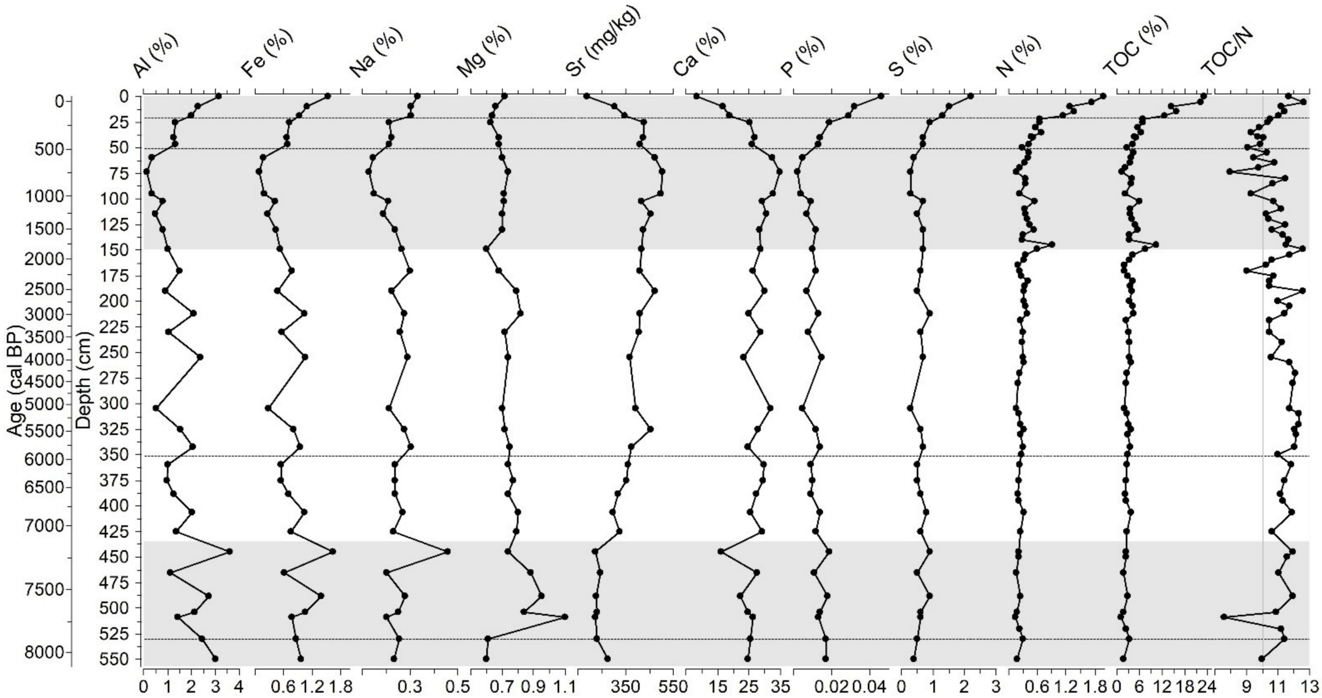

Figure 8. Selected major and trace element concentrations, and N, TOC, and TOC/N values in the sediment core VB-2 from Lake Velo Blato. The grey-shaded and white horizontal bars indicate the changes in sedimentary deposition zones explained in the discussion.

The sediments of Malo Blato have a uniform composition of the main lithogenic elements Al, Ti, K and Fe, which show elevated concentrations in the lower part of the core from 34 to 24 cm, and lower concentrations in the upper part of the core from 20 to 0 cm. Descriptive statistics of elemental concentrations are presented in Table 3. The share of Na has a similar trend, with elevated concentrations in the samples at 8–9 and 0–1 cm, compared to the listed lithogenic elements. The Mg content differs from this trend and shows an increase in concentrations from the lower to the upper parts of the core. The Ca and Sr concentrations are opposite to the concentrations of the lithogenic elements; they are lower in the base of the core (34–24 cm) and higher in the upper parts of the core (20–0 cm). P and S contents show higher concentrations in the lower and upper parts of the core, and are lowest in the middle part of the core (20–12 cm). The concentrations of trace elements in Ba, Co, Cr, Cu, La, Ni, Rb, V, Zn, and Zr show a similar content as the main lithogenic elements, with elevated concentrations in the lower part of the core (34–24 cm) and lower concentrations in the upper part of the core (20–0 cm). Additionally, the Cu content increases slightly in the surface sample (0–1 cm). The share of Cd is higher in the lower parts of the core, especially in sample 24–25 cm, then lower from 20 to 8 cm, and then increasing in the uppermost samples. The Pb concentrations are higher than the rest of the core in the sample at 16–17 cm. The Mo content shows lower values in the middle part of the core (24–12 cm). The Mn content is reversed; the highest concentrations are in the middle part of the core (20–16 cm) and decrease to the surface samples. The Hg concentrations are higher in the lower parts of the core and they decrease in the middle and increase again to the surface samples, except in the 8–9-cm sample, where it has low concentrations.

Table 3. Descriptive statistics of selected major and trace elements from sediments of Velo, Malo, and Kolanjsko Blato (minimum, maximum, mean, median, and standard deviation—SD).

Element	Velo Blato Sediment Core (VB-2)					Malo Blato Sediment Core (MB-1/2)					Kolanjsko Blato Sed. Core (KB-1/1)				
	Min	Max	Mean	Med.	SD	Min	Max	Mean	Med.	SD	Min	Max	Mean	Med.	SD
Al (%)	0.14	3.63	1.53	1.33	0.86	0.57	4.66	1.75	0.86	1.57	2.64	3.99	3.21	3.11	0.42
Ba (mg/kg)	44	165	79	74	25	37	160	73	47	47	75	114	91	89	11
Ca (%)	8.42	34.75	26.17	26.77	5.14	6.77	27.22	20.40	24.64	7.91	17.38	21.85	19.05	18.97	1.39
Cd (mg/kg)	0.1	0.7	0.3	0.2	0.2	0.4	0.9	0.6	0.6	0.2	0.4	0.7	0.5	0.5	0.1
Co (mg/kg)	0.6	7.9	3.7	3.1	1.9	0.7	8.4	3.0	1.3	3.0	8.1	11.9	9.2	8.7	1.2
Cr (mg/kg)	5	80	32	28	16	12	74	30	16	25	43	66	52	51	7
Cu (mg/kg)	1.5	17.6	7.1	6.3	3.6	4.7	12.8	7.4	5.8	2.8	13.5	429.2	104.4	94.2	121.1
Fe (%)	0.09	1.64	0.75	0.72	0.37	0.22	2.43	0.77	0.28	0.84	1.94	2.51	2.20	2.16	0.15
Hg (mg/kg)	0.01	0.06	0.02	0.02	0.02	0.04	0.07	0.06	0.06	0.01	0.06	0.10	0.09	0.09	0.01
K (%)	0.04	0.92	0.39	0.35	0.20	0.16	1.09	0.43	0.23	0.35	0.48	0.75	0.57	0.57	0.08
La (mg/kg)	1.8	21.8	8.7	7.3	4.6	4.4	25.8	10.9	6.4	8.0	13.3	24.4	18.0	17.7	3.6
Mg (%)	0.60	1.10	0.74	0.72	0.10	0.57	0.72	0.65	0.65	0.05	0.67	0.88	0.82	0.84	0.06
Mn (mg/kg)	121	325	236	242	49	63	129	89	87	20	481	748	652	660	68
Mo (mg/kg)	0.10	1.00	0.44	0.40	0.17	0.30	1.90	0.68	0.55	0.46	1.40	3.40	2.09	2	0.52
Na (%)	0.128	0.457	0.247	0.238	0.059	0.491	0.814	0.608	0.555	0.114	0.639	2.073	1.371	1.519	0.461
Ni (mg/kg)	1.3	42.9	18.6	17.0	9.8	3.4	40.2	14.2	6.7	13.8	31.5	43.8	38.2	39.4	3.7
P (%)	0.002	0.046	0.014	0.012	0.008	0014	0.037	0.022	0.021	0.007	0.018	0.060	0.041	0.043	0.013
Pb (mg/kg)	1.0	15.4	5.7	5.1	3.3	9.7	313.0	42.3	10.9	90.3	12.6	30.2	25.1	27.5	6.3
Rb (mg/kg)	2.00	58.90	24.83	22.10	13.86	8	69.80	25.73	12.20	23.52	30.80	55.30	39.56	36.90	7.83
S (%)	0.3	2.2	0.7	0.6	0.4	0.4	2.2	0.9	0.5	0.7	1.6	2.6	2.3	2.4	0.3
Sr (mg/kg)	188	504	360	373	89	127	389	305	365	106	643	1107	985	1012	130
Ti (%)	0.008	0.208	0.081	0.072	0.044	0.034	0.243	0.094	0.052	0.078	0.114	0.182	0.140	0.136	0.022
V (mg/kg)	3	55	27	24	14	8	71	25	11	24	28	58	39	35	10
Zn (mg/kg)	5	61	25	22	12	18	60	29	20	15	52	63	60	61	3
Zr (mg/kg)	1.8	42.7	18.0	16.3	9.8	6.7	56.7	21.2	10.8	19.0	30.7	48.5	37.4	36.9	6.1

3.5. Total Organic Carbon and Nitrogen Concentrations

Concentrations of the total nitrogen (TN) and total organic carbon (TOC) in the sediments of Velo Blato (VB-2) are lower in sediment core between 550 and 150 cm, after which they increase slightly and are the highest from 19 to 0 cm (Figure 8). Nitrogen concentrations in the upper 19 cm of the sediment core are much higher (1–2%) than the rest of the core (0.14–0.68%). In this interval, significantly high concentrations of organic carbon (TOC) are observed (12.58–23.03%). The TOC content is also high in other sediment samples throughout the sediment core from Velo Blato, varying between 1.06 and 7.54%. The inorganic carbon (TIC) content is lowest in the upper 19 cm of the core, where the TOC content is the highest. The TIC values are also low in the 445–446-cm sample, in which the insoluble residue is high. The ratio of organic carbon to nitrogen (TOC/N) varies between 7.60 and 12.63, and in most of the samples, it is higher than 10.

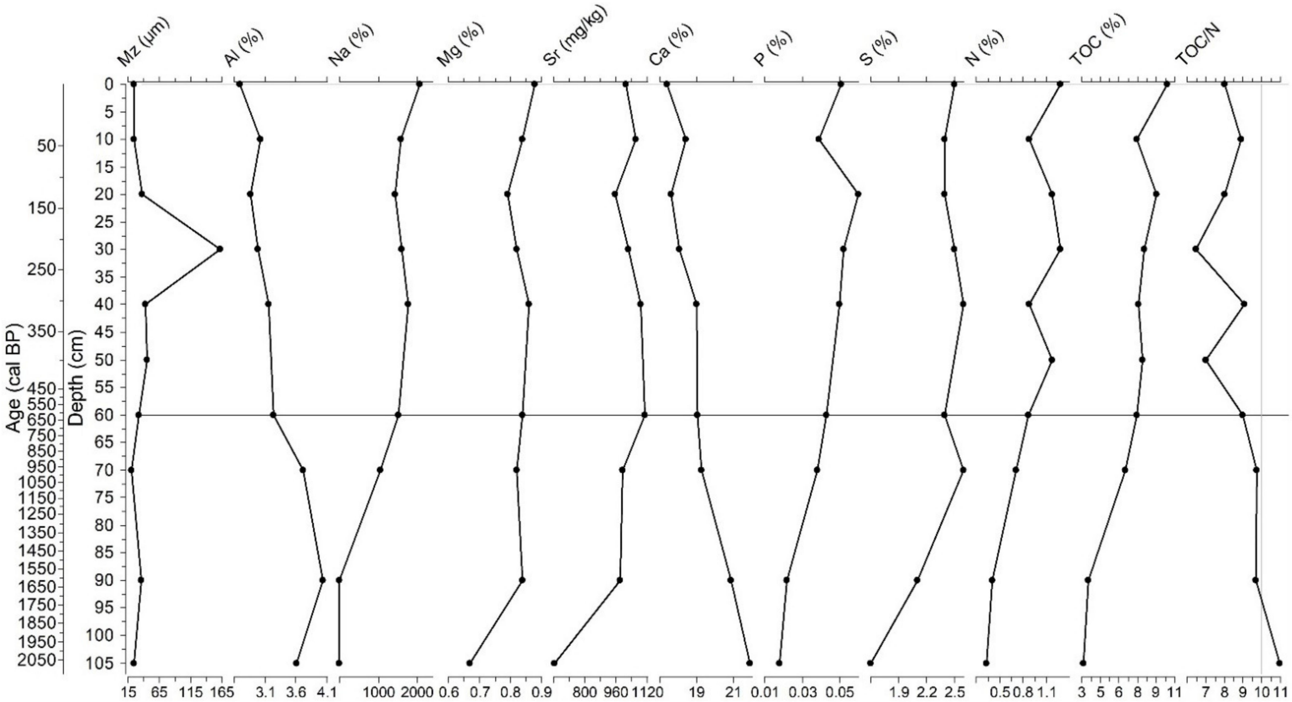

Figure 9. Selected major and trace element concentrations, mean grain size (Mz), and N, TOC, and CN values in the sediment core KB-1/1 from Kolanjsko Blato, with a marked black horizontal line indicating sediment deposition changes.

Nitrogen and total organic carbon increase from the lower parts of the core upwards in the sediments from Kolanjsko Blato (Figure 9). Nitrogen reaches values higher than 0.8 in the upper part of the core from 60 cm upwards. The TOC concentrations are high in all samples throughout the sediment core KB-1/1 (>3%) and show an upward trend from the deeper to the surface samples. The lower TOC values are in the lower part of the sediment core, at 105–90 cm (3.14–3.50%), compared to the higher concentrations from 70 to 0 cm, where it varies from 6.49 to 9.91%. The inorganic carbon (TIC) content is relatively constant, with the lowest values in the uppermost samples.

Malo Blato is characterized by low nitrogen values (<1%), while TOC concentrations are relatively high (2.83–9.72%) in all samples from the sediment core MB-1/2. The TOC content is the highest in the lower parts of the core, from 34–24 cm (8.00–9.72%), which are, at the same time, the samples with TOC/N ratios higher than 10, i.e., between 16.45–17.91. Lower values of TOC than the rest of the sediment core have samples from 20 cm upwards with an increasing trend; although these concentrations are not low at all, the values are higher than 2.6%. The uppermost samples of the sediment core have values between 3.94 and 5.22% (8–0 cm). The values of inorganic carbon (TIC) are lowest in the lower part of the core (34–24 cm), and increase towards the upper part of the core (20–0 cm), and have a trend opposite to the insoluble residue.

3.6. Ostracod Assemblage

The Velo Blato sediment core samples are very rich in ostracods, mollusks, characean stems, and gyrogonites, except for the uppermost (0–20 cm) organic-rich sediment. Several intervals throughout the core are made almost exclusively from gastropods *Bithynia tentaculata* and ostracod shells, which are visible to the naked eye. The most abundant species throughout the core are *Cyprideis torosa* (Jones), *Candona angulata* (Müller), and *Candona* sp., *Limnocythere inopinata* (Baird), *Darwinula stevensoni* (Brady and Robertson), *Cypridopsis vidua* (Müller), and *Cypria ophtalmica* (Jurine), with *C. torosa* being extremely abundant among them. Other notable species, but less abundant, are *Paralimnocythere psammophila* (Flössner), *Pseudocandona marchica* (Hartwig), *Herpetocypris* sp., *Ilyocypris* sp., *Metacypris* *cordata* (Brady and Robertson), *Cypris bispinosa* (Lucas), and *Hungarocypris madaraszi* (Örley). Selected ostracod species are presented in Figure 10.

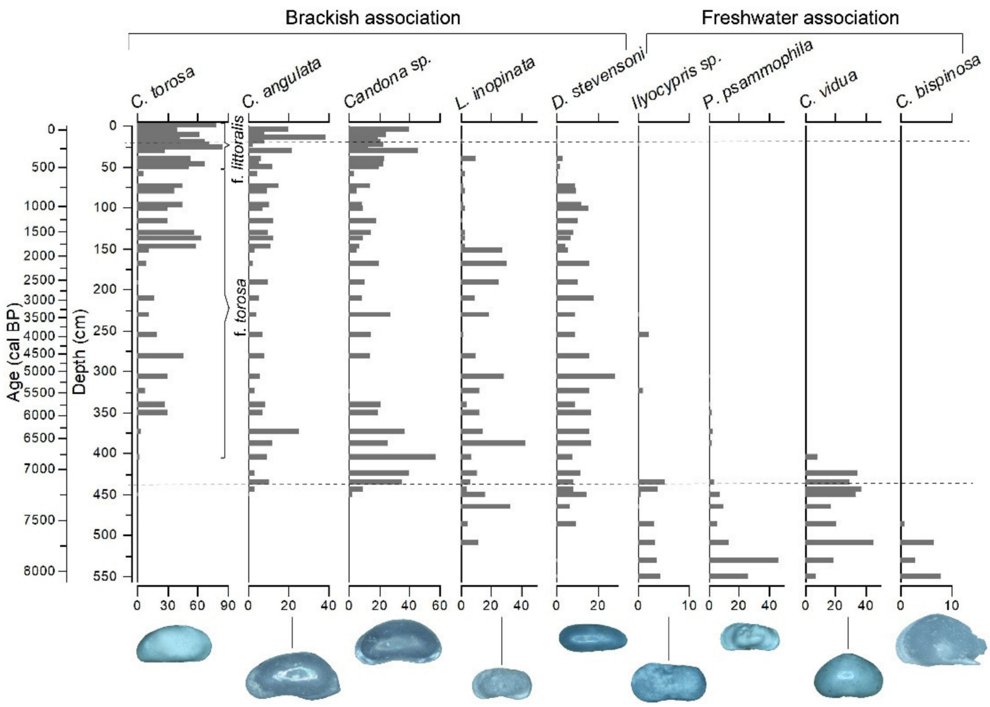

Figure 10. Relative distribution (%) of selected ostracod species in the sediment core from Velo Blato, with their photographs. Three general zones are marked by horizontal dashed lines.

The most dominant species in the lower part of the core (550–435 cm) are *C. vidua* and *P. psammophila*, while *L. inopinata* and *D. stevensoni* are subordinated (Figure 10). *Ilyocypris* sp. and *C. bispinosa* are also present. From 550 to 531 cm, ostracod valves are mostly broken and dominated by juveniles (e.g., *Candona* sp., and *C. vidua*) and fragmented gastropods. Between 531 and 435 cm, valves are well preserved, more adults appear, mollusks such as *B. tentaculata*, *Planorbis* sp., and *Pisidium* sp., and large diatoms (*Campylodiscus* sp.) are present.

The upper part of the core (435–20 cm) shows a higher species richness and the clear dominance of *C. torosa*, *C. angulata*, and *Candona* sp., but also *L. inopinata*, *D. stevensoni*, and *C. ophtalmica* (Figure 10). In several depth intervals (23–24, 48–49, 74–75, and 131–132 cm), the hyperproduction of *C. torosa* (>1500 valves per 1 g dry sieved sediment) was recorded. From 531 to 20 cm, ostracod valves are numerous, and often come as well-preserved carapaces. Good preservation can also be seen in numerous mollusks, especially *B. tentaculata*. Species richness suddenly decreased in the topmost (20–0 cm) darker, organic-rich samples, and only a few valves of *C. torosa* and *C. ophtalmica* dominated. Valves of *C. torosa* are smoothed (forma *torosa*) from their first appearance (435 cm) until 51 cm, when they are dominantly in noded form (forma *littoralis*) to the top of the sediment core.

Samples retrieved from the sediment core from Malo Blato are rich in ostracods in the upper part (20–0 cm), while in the lower part (35–20 cm), ostracods almost vanish. In the lower zone, organic detritus and quartz grains are observed, as well as very fragmented mollusk shells, except for the juvenile gastropods and *Pisidium* sp. Large diatoms were also recognized (*Campylodiscus* sp.). In contrast, the upper zone is calcareous, rich in ostracods, mollusks, and Chara remains. The sample at 12–13 cm contains a fragment of an echinoid spine. The most abundant ostracod species are *Cyprideis torosa* (Jones), *Heterocypris salina* (Brady), *Candona angulata* (Müller), *Candona* sp., and *Herpetocypris* sp. Other noted species are *L. inopinata*, *D. stevensoni*, *P. marchica*, and *H. madarszi*.

Common ostracod species in the sediment core from Kolanjsko Blato are *C. torosa*, *C. angulata*, *Candona* sp., and *H. salina*, which were identified in all samples. There are no significant changes in macro- and micro-faunal composition with depth. Brackish foraminifera (*Ammonia* sp.) and bivalves (*Cerastoderma* sp.) were present throughout the sediment core.

3.7. Radionuclides Activities and Sedimentation Rates

The measurement of anthropogenic radionuclide ^{137}Cs from sediment core profiles can be used as a chronological marker since the radioactive emissions are well known: the development of the nuclear power industry and weapons testing during 1950s and 1960s, and the fallout from the Chernobyl accident [99]. The first significant appearance of ^{137}Cs peak in both sediment cores appeared at a depth of 10 cm (Figure 11), indicating the 1960s, when the emissions of anthropogenic radionuclides occurred due to nuclear weapons testing [99]. The recent peak (4–5 cm) is due to the Chernobyl accident, which produced a radioactive discharge in 1986. Furthermore, residues were observed at a depth of 22 cm in Velo Blato sediments (2.50 Bq/kg) and 16–17 cm in Kolanjsko Blato sediments (38.33 Bq/kg). Down-core mobilization of ^{137}Cs is evident because the oldest measured subsamples from Velo and Kolanjsko Blato (40–41 cm) contain trace amounts of this anthropogenic radionuclide. Concentrations of ^{137}Cs activity in Kolanjsko Blato sediments generally show higher values (12.1 to 48.2 Bq/kg) than Velo Blato sediments (1.5 to 3.9 Bq/kg).

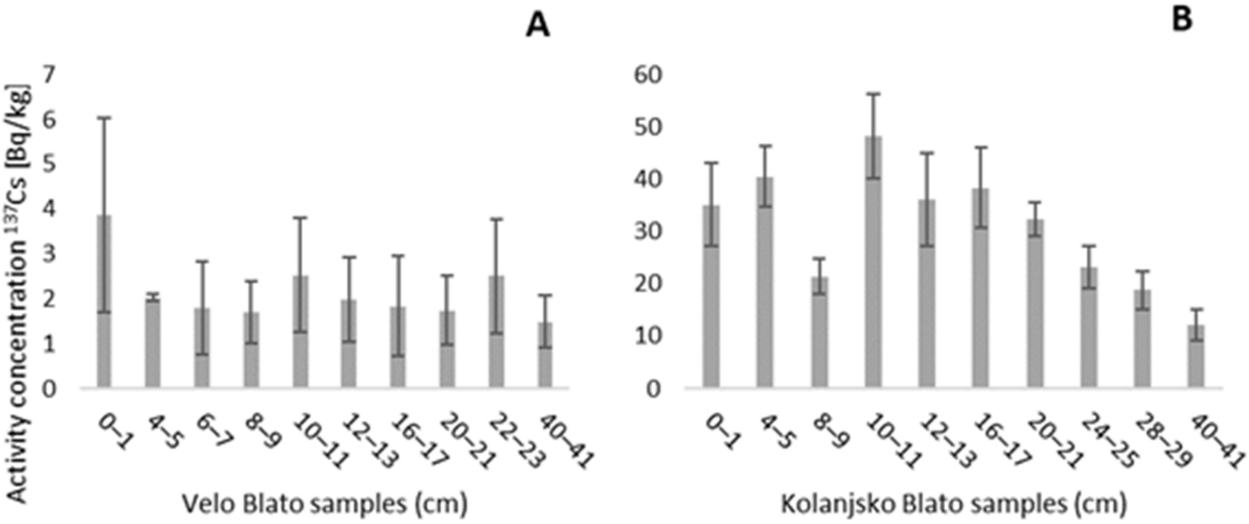

Figure 11. Activity concentrations of cesium radionuclide (^{137}Cs) in sediment core samples from Velo (**A**) and Kolanjsko Blato (**B**).

Similar lower ^{137}Cs activity concentrations were found in Neretva Channel (3.7 to 13.7 Bq/kg) [100]. Lake sediments from Lake Vrana near Biograd contain ^{137}Cs concentrations that vary between 0.3 and 68 Bq/kg [101]. In the sediment profiles from Lake Kozjak and Lake Prošće, the ^{137}Cs activity maximum of 125 Bq/kg at depth 1−2 cm in Lake Prošče, and 131 Bq/kg at depth 4−5 cm in Lake Kozjak, are attributed to the Chernobyl accident in 1986 [102]. Velo Blato sediments have ^{137}Cs activity concentrations similar to the activity values in the sediments from the middle part of the Adriatic Sea (1.3 to 6.0 Bg/kg) [103] and near the Palagruža Island, and the middle and south Adriatic pits (0.22 to 10.42 Bq/kg) [104].

The estimated sedimentation rates in Velo and Kolanjsko Blato are 2.9 mm/yr. Compared to other values from the Adriatic Sea, the stated sedimentation rates are approximately the same; the sedimentation rates determined in the outer part of the Adriatic Sea are 5 mm/yr [103] and 3.1 mm/yr [104] in the Jabuka pit, while in the area of Palagruža and the south Adriatic pit it is 1.8 mm/yr [104]. In the Krka River Estuary and Lake Prokljan, rates vary between 1 and 4 mm/yr [105]. In the sediments from Lake Vrana near Biograd, sedimentation rates are 6.4 mm/yr in the NW part of the lake and 4.2 mm/yr in the SE part of the lake [101]. In front of the Neretva River mouth, the sedimentation rate is 6 mm/yr and 4 mm/yr in the Neretva channel area [100].

4. Discussion

4.1. Paleoenvironmental Reconstructions of Lake Velo Blato and Wetlands Malo and Kolanjsko Blato

The sediment core from Velo Blato (VB-2) comprises lake sediments in the length of 554 cm. The base of the core, from 554 to 568 cm, is made of limestone fragments that present weathered carbonate bedrock on which lake sediments were deposited. This implies the lake formation at the depth of the transition from bedrock into lake sediments, which yields the time of 8100 cal yr BP. The relative sea level (RSL) 10,000 years ago was approximately 40-m lower than today [106]. The coastline was further away from Velo and Malo Blato; therefore, the seawater had no influence on their ecosystem, nor on the Kolanjsko Blato. The paleoshoreline of the eastern Adriatic coast in the area of Pag Island at approximately 9000 years BP was more distant (seaward) from the present shoreline, and the vast area was dry land (Figure 12). At the time of the Early Holocene lowstand on the eastern Adriatic coast, Velo and Malo Blato exist as lakes, but as geomorphological depressions, karst poljes (Figure 12A). During the Early Holocene, the sea level rose rapidly, and at about 8000 years BP, it was approximately 10-m lower than today [9,106,107]. The rising sea level enabled the formation of a freshwater lake in Velo Blato at 8100 cal yr BP (Figure 12B).

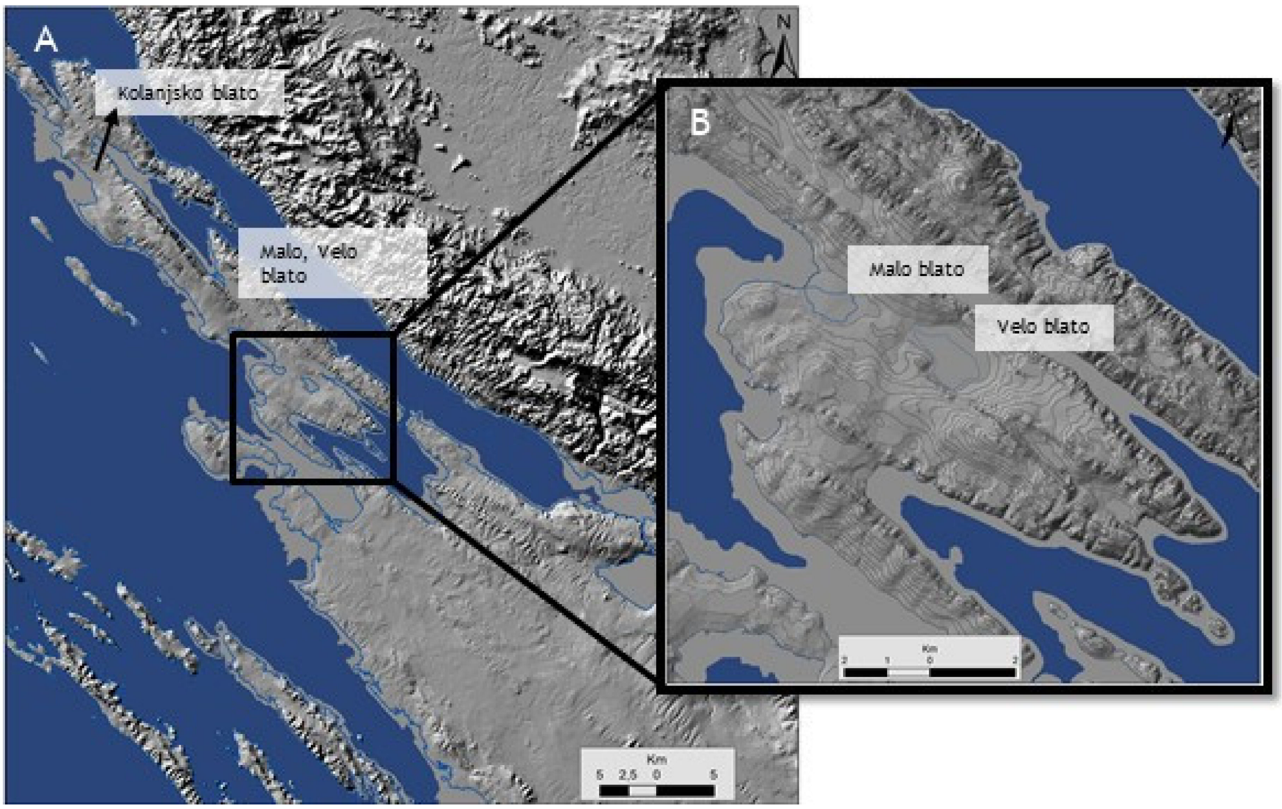

Figure 12. (**A**) Paleoshoreline of the eastern Adriatic coast at approximately 9000 years BP (20-lower than today); (**B**) detailed locations of Malo and Velo Blato karst poljes—basins.

Coastal areas of Pag Island on the EAC are shaped under the influence of the Late Pleistocene–Holocene sea-level rise [108]. The formation of the present-day coastline is the result of post-Last Glacial Maximum (LGM) sea-level rise [8,109,110]. The EAC coastal zone shows typical morphologic features associated with the chemical dissolution of carbonates, water rich in carbonate ions (hard water), and the intrusion of seawater through the karstified underground, inherited from the karstification processes.

The lake sedimentation in Velo Blato began 8100 years ago (from 554 cm upwards). Generally, lake sediments in Velo Blato are characterized by lake carbonate sedimentation due to the saturation of lake water with carbonate ions resulting from the karst environment and calcareous bedrock, in which the precipitation of endogenic calcite from the lake-water column predominates. Photosynthetic processes enhance calcite precipitation on the lake bottom caused by aquatic plants (algae and macrophytes), due to the water's carbon dioxide consumption and increased pH [111]. The more productive the lake, the more endogenic calcite is precipitated, while in contrast, the decomposition of organic matter leads to the formation of CO_2, the pH decreases, and calcite dissolves [1]. The solubility of calcite decreases with increasing temperature; therefore, increased water temperature promotes calcite precipitation. In the lower part of the core (554–435 cm), which corresponds to the period between 8100 and 7100 cal year BP, lithogenic elements Al, Fe, K, and Na, which are bound to the siliciclastic material, are slightly increased. In this interval, in addition to the carbonate minerals calcite and aragonite, dolomite and related elevated concentrations of magnesium are observed in the samples, except in the base of the core. Dolomite is defined as a detrital mineral, and this indicates erosional processes and the input of the material from the catchment into the lake. At first, in addition to carbonate lake sedimentation, a significant portion of material with elevated content of Al and other siliciclastic elements were deposited, followed by the carbonate lake sedimentation alongside detrital material with dolomite. The interval with the magnetic susceptibility peak corresponds to the peaks of Al and other siliciclastic elements and higher clay mineral contents, while the calcium content is lower. Erosional input from the lake catchment area can also be inferred from the micropaleontological data. Ostracod valves in the lower part of the core (531–550 cm) are represented dominantly by juveniles, while adult valves are often poorly preserved. This is especially the case with some large species, e.g., *H. madaraszi* and *Herpetocypris* sp., as well as with gastropod shells. A large number of juvenile valves or a low adult/juvenile ratio is often used as an indicator of a dynamic environment [112,113], in which juvenile ostracod valves are easily transported away by waves and streams. In contrast, a higher adult/juvenile ratio indicates a more stable environment, where both juvenile and adult valves can be preserved, and thus represents an autochthonous assemblage. A higher number of adults and juveniles appear after 531 cm and continue throughout the core. The most dominant species from 550 to 425 cm are *C. vidua* and *P. psammophila* (Figure 9), and they occur together with *L. inopinata*, *D. stevensoni*, *Ilyocypris* sp., and *C. bispinosa.* Although most of them can tolerate a small increase in salinity, these species thrive in freshwater environments. The predominance of *C. vidua* (maximum salinity 10 ‰, prefers lakes and ponds, [95]) and *P. psammophila* (so far only recorded from small freshwater lakes and pools [95]) point to the development of a small lake.

In the next phase of the Lake Velo Blato evolution, from 7100 to 1800 cal year BP (435–150 cm), the content of lithogenic elements slightly decreased, and calcium and strontium concentrations increased. Magnesium-calcite was recorded as a mineral phase, alongside quartz, while muscovite/illite appeared as an accessory mineral phase. Unlike endogenic carbonate formation that depends mainly on biological processes, authigenic carbonates, such as Mg-calcite, result from specific abiotic conditions in the lake, and seem to be a common feature in the sediments of lakes with high salinities [111]. The sediment runoff from the catchment decreased, while the deposition of endogenic Mg-calcite characterizes carbonate precipitation. The nitrogen and total organic carbon show relatively low and constant values during this period. The organic carbon to nitrogen (TOC/N) ratio is higher than 10, which indicates a terrestrial source of organic matter [114,115] throughout this period of lake evolution. Slightly lower values of TOC/N occurred between 3900 and 3100 cal year BP, and by the end of this phase, between 2400 and 2000 cal yr BP, the values were the lowest, at 2200 cal year BP (<10). In these periods, lowering the TOC/N ratio indicates algae's significant influence to the dominance of vascular plants and terrestrial origin of organic matter [114]. The significant change in ostracod assemblage occurred from 7100 cal yr BP, and is marked by the appearance of brackish ostracod species, the most prominent being *Cyprideis torosa*, a euryhaline species. This is often used as an indicator of more saline conditions, especially in the marginal marine environments that were influenced by the Holocene sea-level rise, such as coastal lakes, lagoons, marshes, and estuaries [116–118]. The species is known to tolerate a wide range of salinities, from 0.5 to more than 60‰, with a reported optimum of 2–16.5‰ [95]. It is accompanied by *C. angulata*, which prefers slightly brackish conditions, and is often found in coastal lakes with *C. torosa* [95]. At approximately 6000 cal year BP (355 cm), a significant increase in the relative abundance of *C. torosa* occurred, and it became the dominant species in the ostracod community, which coincides with the increase of Sr content. At the same time, freshwater species *C. vidua, P. psammophila*, *Ilyocypris* sp., and *C. bispinosa* decrease, while *D. stevensoni* and *L. inopinata* are still well distributed. *C. angulata* and *Candona* sp. occur earlier than *C. torosa*, between 450 and 350 cm. However, the presence of oligohaline species, which have a much smaller range of salinities (e.g., from 0 to 25‰ for *L. inopinata*, and from 0.5 to 15‰ for *C. angulata* [119]) suggest moderate saline conditions in the lake [118]. This is supported by the presence of freshwater mollusks *B. tentaculata*, *Planorbis* sp., and *Pisidium* sp.

Freshwater bodies are influenced by dynamic groundwater, especially in coastal karst terrains, where seawater is connected. Seawater intrusions into the coastal Dinaric karst aquifers are investigated on the islands on the Dalmatian coast [120,121]. The groundwater table declines towards the sea, and freshwater overlies saltwater, penetrating the aquifer at a certain depth, in a wedge-like form. On smaller islands, an aquifer is partially formed as a lens of fresh and brackish water above seawater, according to the Ghyben–Herzberg principle of gravitational equilibrium [122,123]. This says that the depth below sea level at which the freshwater–saltwater interface (the halocline) occurs is related to the elevation of the water table above sea level and the density of the fresh (1.0 g/cm^3) and salt (1.025 g/cm^3) waters, respectively [5]. Since the Ghyben–Herzberg law describes the sharp interface contact of two fluids (freshwater and seawater), in natural conditions—due to the groundwater dynamics, chemical mixing, and tide effects—that contact is not sharp, and the model can be taken only as a rough estimation. A relatively wide transition (or mixing) zone is formed between freshwater and seawater, making part of the aquifer brackish [121]. Although the Island of Pag is one of the largest Adriatic karst islands, most aquifers are separated and relatively small due to their high indentation. The sea-level rise during the Holocene in the Adriatic Sea changed the aquifer boundary conditions, which controlled the fresh and saline groundwater flows. The scheme of the seawater intrusion into freshwater in control of the sea-level rise is presented in the example of Velo and Malo Blato in the last 10,000 years (Figure 13A–C). Three phases of lake development in Velo Blato are presented in the sketch (the first two were already mentioned): (A) Early Holocene, at ~10,000 years ago, when the sea level was much lower than today (~40 m) and seawater had no impact on the waters of Velo and Malo Blato, and they existed as geomorphological depressions or karst poljes, under the strong influence of erosional processes and with no sediment preserved (all the material was washed away from the polje); (B) Early–Middle Holocene transition, at 8100 years ago (the sea level was ~10 m lower than today), when the rising sea level caused the formation of the freshwater lake in Velo Blato and lake carbonate sedimentation began on karstic weathered bedrock; and (C) Middle Holocene, at 7100 years ago, when the further sea-level rise influenced the movement of the salt- and freshwater boundary towards the underground of Velo Blato and resulted in the influence of brackish water on the sediments of Velo Blato from that period onward, especially from 6000 cal yr BP, as well as lake-level deepening in Velo Blato. The saltwater intrusion and saline groundwater influence on lake sediments in Velo Blato are evident by the geochemical and ostracod proxies. According to the geomorphological characteristics of Velo Blato, the lowest relief around the lake is a 5-m high ridge towards Malo Blato. This is also the height over which the lake level did not exceed. The known water depth of the core VB-2 in Velo Blato (2.75 m), and a sediment length of 4.25 m under the sea-water influence, lead to the conclusion that the maximum possible depth of the lake in Velo Blato could be approximately 12 m.

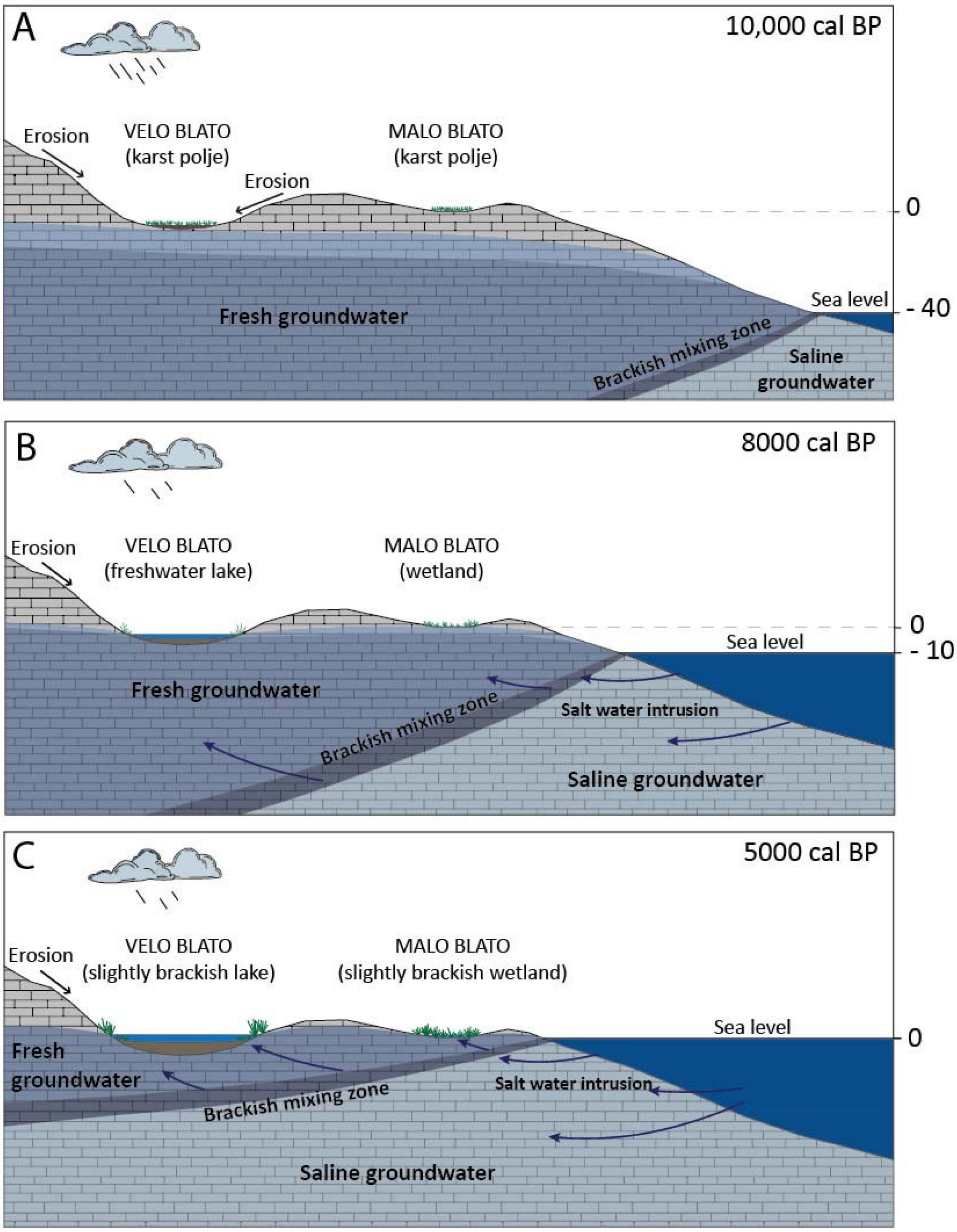

Figure 13. Schematic presentation of seawater intrusion into freshwater coastal lakes and wetlands, caused by the sea-level rise, on the example of Velo and Malo Blato in the last 10,000 years. (**A**) Velo and Malo Blato as karst poljes during the Early Holocene lowstand. (**B**) Sea-level rise in the Adriatic Sea resulted in rising the groundwater level and the formation of a freshwater lake in Velo Blato at approximately 8100 cal year BP, and the formation of a wetland in Malo Blato. (**C**) Saltwater intrusion and saline groundwater influence on lake sediments in Velo Blato in Middle Holocene at 5000 cal year BP (started from 7100 cal year BP), resulting in brackish environments in Lake Velo and wetland Malo Blato.

The reconstruction of sea-level influence during the Holocene in lake sediments in Velo Blato enabled the sea-level curve reconstruction in the Adriatic Sea. The time of marine influence on the lake sedimentation is determined when the sea level rose enough to infiltrate into the lake sediments in Velo Blato. At approximately 7100 cal year BP, the brackish ostracods are present, and the geochemical signal indicates marine influence; therefore, that is the apparent age when the sea level was ~7-m lower than today (Figure 14). The data points from Velo Blato are compared with other studies on the eastern Adriatic coast [14–17,48,49], and it fits well into the relative sea-level curve in the Adriatic Sea [107] and global eustatic sea level curve [106].

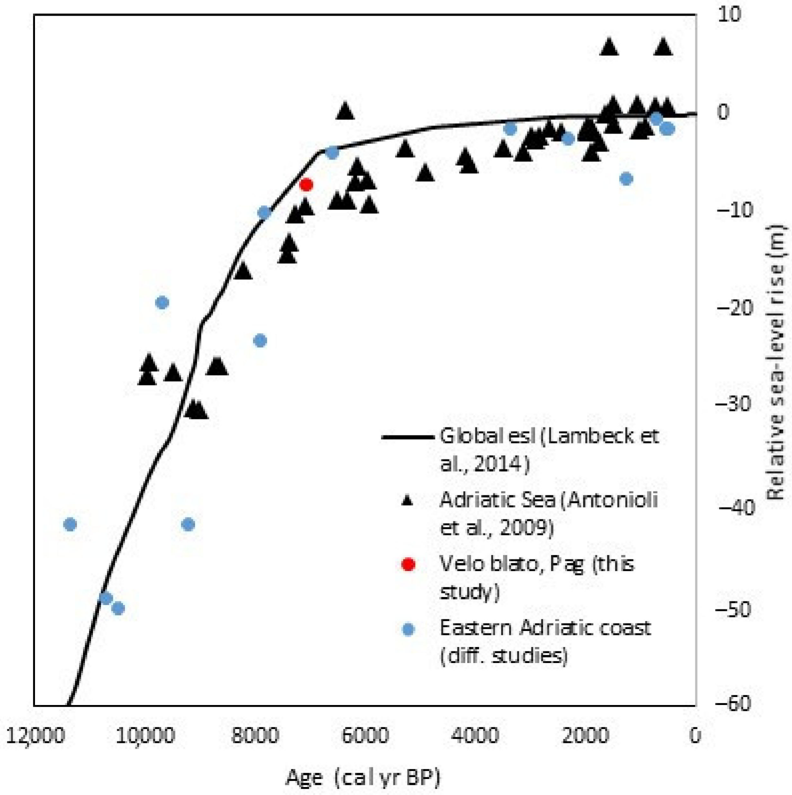

Figure 14. Relative sea-level rise during the Holocene in the Adriatic Sea [107] in relation to the global eustatic sea-level (esl) curve [106], and index points from this study (red dot) and other studies on the EAC [14–17,48,49].

In the Late Holocene, at 1800 cal year BP (150 cm), the next phase is determined, marked by the increase of TOC and N content in lake sediments from Velo Blato, especially at 1750 cal year BP at the beginning of this period. Between 1800 and 600 cal year BP (150 and 50 cm), there is an evident decreasing trend in lithogenic elements (Al, Fe) and somewhat lower values of TOC/N compared to the rest of the core. At the same time, an increasing trend is evident in carbonate elements (Ca, Sr) and TIC. This is accompanied by metal accumulation, especially lead, copper, and zinc (Figure 15). Additionally, the increased number of brackish ostracod species *C. torosa* and *C. angulata* indicate higher salinity. This period is, therefore, characterized by higher water salinity and carbonate precipitation. This indicates a warmer interval, which is approximately equivalent to the Roman (0–800 AD) and Medieval Climate Anomaly periods (800–1400 AD) [124], with a global increase in temperature [125]. During this period, accelerated sea-level rise is identified in the central and northern part of the eastern Adriatic Sea, based on the algal rim morphology and the tidal notches positions [53,54]. From approximately 750 cal year BP (74 cm) upward, calcite occurred as the dominant mineral phase, in contrast to Mg-calcite deposited until that period. Together with the Sr decrease, this indicates the decrease in salinity. Nutrient elements P and S have elevated concentrations in the last 600 years (sediments from 50 cm upwards). This period, from 600 to 200 cal year BP, coincides with the cold and humid period of the Little Ice Age (LIA; 1300–1800 AD; [124]). This is supported by the increased siliciclastic input of lithogenic elements (Al, Fe), introduced into the lake by increased precipitation and sediment runoff. This is followed by the changes in the valve morphology of *C. torosa* from smooth (forma *torosa*) to noded (forma *littoralis*), which points to the changes in salinity, i.e., f. *torosa* is indicative of more saline conditions, while f. *littoralis* prefers reduced salinity [95]. The LIA period is identified in the eastern Adriatic as a relatively stable sea level period [53,54]. Increased precipitation and sediment input correlate well with this more humid phase in the central Mediterranean, evidenced in Lake Butrint, Albania [12], and Lake Dojran [126,127].

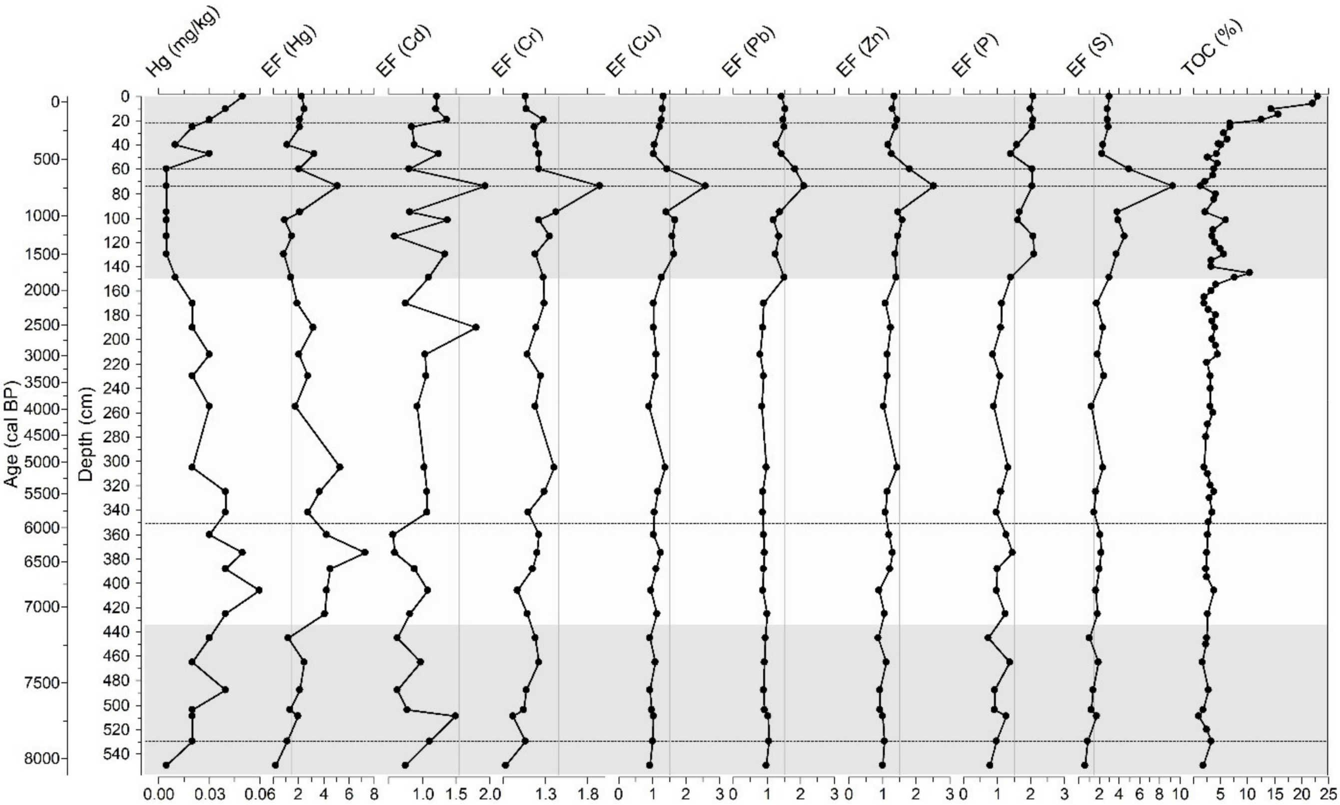

Figure 15. Enrichment factors (EFs) for Hg, Cd, Cr, Cu, Pb, Zn, P, and S, as well as concentrations of Hg and TOC in the sediment core from Velo Blato.

Recent times, i.e., the last 200 cal yr BP (after 1800 AD; interval 21–0 cm), are characterized by significantly higher P, S, N, and TOC values. The concentrations of carbonate elements (Ca and Sr) and TIC decreased. At the same time, the proportions of organic carbon (TOC) were the highest (12–23%). An increased accumulation of organic matter led to anoxic conditions: a high production of CO_2 due to the breakdown of organic matter in sediments and a decrease of water pH, which dissolved calcite reaching the lake bottom. These processes are responsible for the seemingly lower concentrations of calcite and carbonate elements (Ca, Sr) and the elevated concentrations of lithogenic elements. In reductive conditions, the formation of framboidal pyrites, which occurred in significant amounts in this interval, is characteristic of being rich in organic matter. High TOC indicates an increased primary production and development of aquatic plants (algae and phytoplankton) and macrophytes and eutrophication in the lake. Changes in nutrient status influenced the ostracod relative and absolute abundances. Samples were rich in organic detritus, plant remains, and seeds, but poor in calcareous microfossil remains, and only a few ostracod valves of *C. torosa* and *C. ophtalmica* were found in the topmost sample. High TOC and nutrient elements versus a low Ca content point to the anoxic conditions in recent sediments of Velo Blato, which would promote the dissolution of calcified ostracod valves [118,128]. During the fieldwork in spring and summer, a load of macrophyte algae was detected on the lake bottom, and recent ostracod valves were detected on calcified

Chara stems. Therefore, low ostracod content in the uppermost part of the sediment core from Velo Blato could be related to the periodically anoxic conditions in that part of the lake. The exclusive presence of *C. torosa* and *C. ophtalmica* in the topmost sample (0–4 cm) of organic-rich sediment is due to their known H_2S and hypoxia tolerance [118,128,129].

The paleoenvironmental reconstruction of Kolanjsko Blato is based on a recovered lake sediment core in the length of 107 cm, which holds the record of the last 2050 years. Kolanjsko Blato is a brackish wetland, due to its proximity to the sea through the karstified carbonate ridge and a seasonal surface connection in the SE edge through the Rogoza canal. The influence of the seawater on the wetland is evident in the measured high surface water salinities (EC = 4.88 to 9.8 mS/cm, Cl- content = 2700 to 6257 mg/L, as well as other geochemical parameters), which are the highest in the central and eastern part of the Kolanjsko Blato (Table 1). These values are higher than measured values in both Velo and Malo Blato (Table 1). Consequently, genuine brackish water associations appear in lake sediments *C. torosa*, *C. angulata*, and *H. salina*, accompanied by the brackish foraminifera *Ammonia* sp., and marine bivalve *Cerastoderma* sp. Since no significant changes in ostracod communities were detected by qualitative analysis, Kolanjsko Blato existed as a relatively shallow brackish coastal wetland during the last 2050 years. A relatively high content of sand (avg. 44%) in silty sediments (avg. 50%) indicate a somewhat dynamic depositional environment. The geochemical composition of lake sediments shows depositional changes from 650 cal yr BP (60 cm). A slightly higher content of siliciclastic elements in the lower part of the core indicates higher detrital input and sediment runoff between 2050 and 650 cal BP. In the last 650 years, the content of TOC and nutrients (N, P, S), and heavy metals (Cu, Hg, Pb, and Zn) increased due to the enhanced organic matter accumulation. The TOC concentrations are generally high in the Kolanjsko Blato sediment core (>3%) and increase up to 9% from the 650 cal yr BP, while the TOC/N values turn lower than 10. Thus, the source of the organic matter was dominantly algal (autochthonous) and the result of the primary lake production [114]. The lower Ca content, at the same time, was the result of the calcite dissolution in the water column before it reached the lake bottom due to the increased CO_2 and decreased pH of the water, which led to apparent anoxic conditions. TOC concentrations in Kolanjsko Blato lake sediments are quite high (3.1–9.9%; avg. 7.05%), compared to Velo Blato lake sediments (1.06–10.5%; avg. 3.6%), except for the upper 20 cm, where it is higher than 12% (12.6–23%), and the upper part of the sediment core from Malo Blato (2.97–5.22%; avg. 3.48%). Such high TOC values (~3–10%; avg. 6.15%) were recorded only in the laminated lake sediments of Lake Veliko on the Island of Mljet [16,27]. In other lake carbonate sediments, such as Lake Vrana near Biograd [23], Bokanjačko Blato [26], and Lake Crniševo in the Baćina Lakes [19], the TOC concentrations are lower than <2%. Sediments from Kolanjsko Blato are enriched in ^{137}Cs compared to the sediments from Velo Blato, which could be related to the higher organic carbon content in the Kolanjsko Blato sediments, as organic matter is essential for ^{137}Cs radionuclide accumulation [130,131]. Similarly, the accumulation of artificial ^{137}Cs is determined in the Neretva River mouth in sediments with higher organic matter content [100].

The Malo Blato wetland is characterized by the unique geomorphological setting, in which the permanent lake makes only the small central part of the area, connected to the sea with an almost 0.5-km long artificial canal. Therefore, the water salinity is reduced compared to the sea, with a surface water electrical conductivity value of 3.8 mS/cm, and a Cl- content of 1898 mg/L (Table 1), which are still higher than in Velo Blato, but lower than in Kolanjsko Blato. The broader area of the Malo Blato wetland is covered with dense vegetation characteristic of swamp and peat. This corresponds to dark, almost-black organic soils surrounding this small lake in Malo Blato. The lower part of the sediment core from lake Malo Blato (34–24 cm) is composed of these soils, high in TOC (~8%) and lithogenic elements (Al, Fe). The lake formation is observed from 20 cm upwards, indicated by grey lake sediments, with higher contents of Ca and calcite, and being rich in ostracods and gastropods. The lake formation is connected with the sea level rise during the Holocene and the influence of the seawater on the lake sedimentation, as previously described in

Figure 13. Ostracod assemblage in the upper part of Malo Blato sediment core showed the dominance of *C. torosa*, accompanied by *H. salina* and *C. angulata*. *Heterocypris salina* prefers small and slightly salty coastal water bodies [95]. The presence of freshwater species *L. inopinata*, *D. stevensoni*, and *P. marchica* is also observed. Additionally, the TOC/N values are lower than 10, indicating organic matter's algal origin [114]. Nutritive elements P, N, and TOC increase upwards to the surface samples, and indicate more eutrophic conditions in lake Malo Blato in the recent period.

4.2. Evaluation of Metal Enrichment

Potentially toxic elements, i.e., metals (Cd, Co, Cr, Cu, Hg, Mo, Ni, Pb, and Zn) analyzed in sediment cores from Velo, Malo, and Kolanjsko Blato show similar concentrations to marine and lake sediments along the eastern Adriatic coast [14,15,19,26,103]. Slightly elevated concentrations of Cr and Ni in the sediments reflect source material in Croatian karst (terra rossa and flysch) and its geological origin [132]. The Enrichment Factor (EF) represents a useful tool for estimating the degree of anthropogenic heavy metal pollution and the status of environmental contamination. This is confirmed by the EF values for of metals, with EF medians between 0.5 and 1.4, since the reference threshold for natural/anthropogenic origin of the metals is 1.5 [93]. Elements Cd, Cr, Cu, P, Pb, and Zn are considered here with their EFs presented in the chronological framework for sediment cores from Velo and Kolanjsko Blato, while an in-depth framework is presented for sediments from Malo Blato. Deviations in terms of elevated concentrations from the geogenic origin and natural variations in the concentration of elements originating from lithological units, and their weathering products in the catchment areas of the studied lakes, are found only in few samples for elements Cd, Cr, Cu, Pb, and Cu, and for P and S as nutrients. The EF of Cd is elevated in two intervals (190–191 and 75–76 cm), while the EFs for Hg, Cr, Cu, Pb, and Zn are elevated in the interval between 130 and 60 cm. The P and S EFs increase from the depth of 149 cm upwards. The distributions of metals appear consistent, and variations are the effect of dilution caused by enrichments of carbonate. High organic matter contents and TOC values in the upper part of the lake sediments, from 150 cm upward, coincide with the Pb, S, and P accumulation. This interval corresponds to the period between 1800 and 600 cal year BP (150–60 cm), known as the Roman and Medieval Climate Anomaly periods. The Roman period lead enrichment is recorded in Lake Vrana sediments on the Island of Cres [103].

The Cu, Pb, P, and Zn concentrations are elevated, and the Efs are greater than 1.5 in the upper parts (60–0 cm) of the sediment core from Kolanjsko Blato, which corresponds to the period of the last 650 cal yr BP. The surface sample is significantly enriched with Cu. They can be attributed to the anthropogenic activities in the vast catchment near the Kolan settlement (Figure 16). High total organic content in the sediment core from Kolanjsko Blato, especially in the upper 60 cm where it is >6%, contributes to these sediments' metal accumulation. In Malo Blato sediments, the enrichment of Cu, P, Pb, and Zn is evident in the upper 20 cm of the sediment core, with the lake formation in Malo Blato. This interval is also rich in TOC content (~3–5%), and the enrichment could be attributed to the organic matter accumulation in the lake sediments. Higher values of Pb than the rest of the sediments from the core show the sample at 16–17 cm, which is also a very coarse sample in terms of grain size. We propose that this is a consequence of bird hunting while using a shotgun and lead bullets, which are commonly used in such wetland habitats in the northern Adriatic coast [91,133], and has been recorded along the EAC in sediments from marine ponds on the Island of Cres [14]. Malo Blato was proclaimed an ornithological reserve in 1988; therefore, hunting was probably carried out in the wetland area until that period, which resulted in the accumulation of lead recorded at a depth of 16 cm. Trace elements in lake sediments from the Lake Kuti and the wetland area of the Neretva River delta indicate a non-contaminated deltaic lake environment [57,134]. The metal enrichments of Pb, Cu, Zn, and Sn in sediments is identified in one location of the Neretva River delta, which is connected with expanded agricultural activities [65].

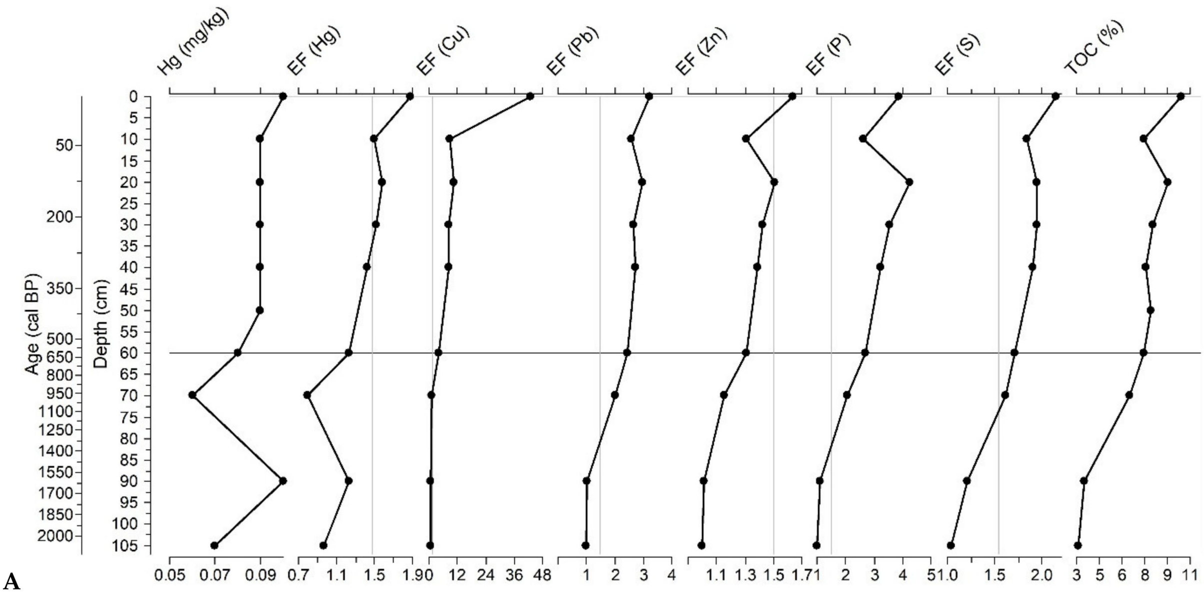

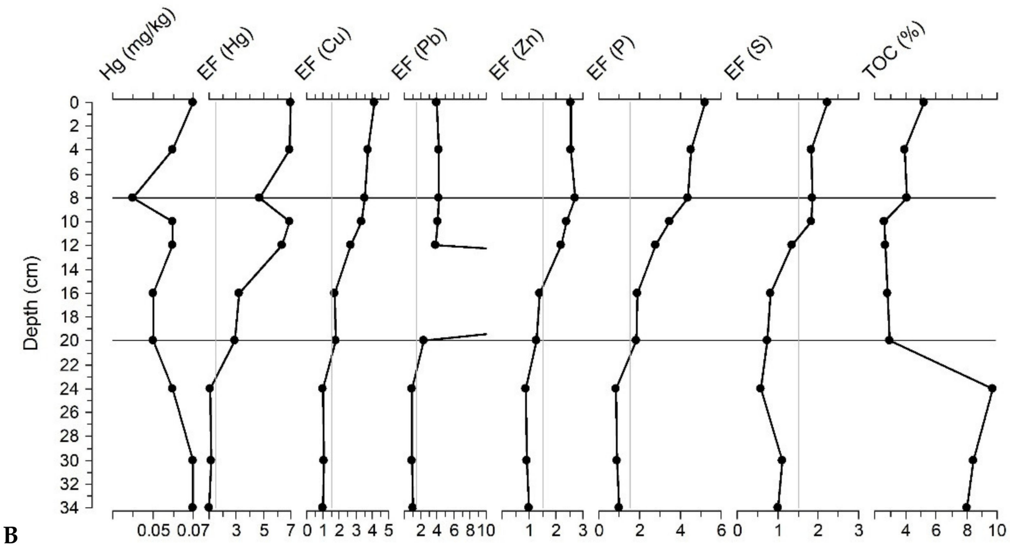

Figure 16. Enrichment factors (EFfs) for Hg, Cu, Pb, Zn, P, and S, as well as concentrations of Hg and TOC in the sediment core from Kolanjsko Blato in depth and age (**A**) and Malo Blato in depth (**B**). Note the reduced maximum value for EF (Pb) to 10 in the Malo Blato sediment core, to emphasize the slight upward-increasing trend, because the value in the interval 16–18 cm is significantly higher (~70).

The Hg concentrations in sediments from Velo Blato are mostly low and vary between 0.01 and 0.06 mg/kg, except in high carbonate sediments, where it is even below the detection limit (<0.01 mg/kg). Higher values (0.04–0.06 mg/kg) appear in the lower and upper parts of the sediment core. The same is for sediments from Malo Blato, where the higher values are 0.06–0.07 mg/kg. In Kolanjsko Blato, the Hg concentrations are slightly higher (0.09–0.1 mg/kg) throughout the sediment core. These values correspond to natural background Hg values of karst soils in the Dinaric-coastal region (median value 0.08 mg/kg) as possible natural sources from catchments karst soils [132]. The similar Hg concentrations are recorded in sediment samples from Lake Prokljan as part of Krka River Estuary [66] and in Lake Veliko on Mljet Island [61], while the increased values from industrial sources are recorded in marine sediments from Šibenik Bay [66] and Kaštela Bay [135]. Additionally, the Hg total concentrations in Velo, Malo, and Kolanjsko Blato are slightly higher than the Hg content in marine sediments from Palagruža, middle, and south Adriatic depressions [19].

5. Conclusions

Lake sediments in Velo Blato on the Island of Pag archived valuable information about lake formation and the development of the area, which is perceived in comparison to the lake sediment deposition in the wetlands of Malo and Kolanjsko Blato. Significant changes in Lake Velo Blato occurred in relation to sea-level changes during the Holocene. In the Early Holocene, Velo and Malo Blato existed as karst poljes without sedimentation, followed by the freshwater lake formation 8100 years ago, due to the rising sea and groundwater levels. The brackish environment in Lake Velo Blato was established from 7100 cal year BP. Further marine transgression caused a more saline environment and the lake-level deepening in Velo Blato during the mid-Holocene. The sediment characteristics clearly indicate warmer periods of the Roman period (0–800 AD) and Medieval Climate Anomaly (800–1400 AD). A decrease in salinity from 600 to 200 cal year BP coincides with the cold and humid period of the Little Ice Age (1400–1800 AD). Increased precipitation and sediment runoff correlate well with this more humid phase in the central Mediterranean. Higher primary production and eutrophication have been evident in the last 200 years. Kolanjsko Blato archives the last 2050 cal yr BP, when it existed as a relatively shallow brackish coastal wetland. In the last 650 years, the organic carbon is accompanied by the heavy metals (Cu, Hg, Pb, and Zn) and ^{137}Cs radionuclide accumulation. A short sediment core from Malo Blato contains the record of lake formation in Malo Blato wetland, which underwent the transition from karst polje and terrestrial soil to the slightly brackish wetland probably during the Early Holocene (not dated).

The studied shallow lake and wetlands have a complex paleo-geographic history related to mid-Holocene sea-level rise, from a polje in a typical karst environment, through freshwater and brackish sedimentation, and more recently eutrophication, to changes in drainage and groundwater abstraction. The study highlights the influence of Holocene sea-level rise on lowland areas in the eastern Adriatic coast and its importance on freshwater lake formation. Lake and wetlands gradually became brackish environments due to the marine intrusion into the groundwater. In addition, analyses allow the sea-level curve reconstruction on the eastern Adriatic coast, which is identified in Lake Velo Blato as 7-m bsl at 7100 cal year BP.

The environmental changes documented in the studied lakes have broader implications elsewhere along the eastern Adriatic coast, as well as in other coastal karst environments, both for the formation of existing lakes as well as paleolakes in karst basins, of which many have been flooded by late-glacial raising sea levels.

Author Contributions: All authors contributed to the study conception and design. Sample preparation, data collection and analysis were performed by N.I., S.M., I.I.F., O.H., M.Š.M., B.P., J.T. and T.M. The first draft of the manuscript was written by N.I., S.M. and I.I.F., and all authors commented on versions of the manuscript. All authors have read and agreed to the published version of the manuscript.

Funding: This research was funded by Public Institution Natura Jadera, Zadar County, Croatia, contract number 3902/20.

Institutional Review Board Statement: Not applicable.

Informed Consent Statement: Not applicable.

Data Availability Statement: Exclude this statement.

Acknowledgments: The authors would like to thank Marko Copić, Natalia Šenolt, and Hrvoje Burić for fieldwork assistance during the drilling survey, and Ana Maria Heski for grain-size analysis. We are grateful to Croatian Waters and Daria Čupić for providing the water chemistry results from the water pumping station of Velo Blato.

Conflicts of Interest: The authors declare no conflict of interest. The funders had no role in the design of the study; in the collection, analyses, or interpretation of data; in the writing of the manuscript, or in the decision to publish the results.

References

1. Last, W.M.; Smol, J.P. An Introduction to Physical and Geochemical Methods Used in Paleolimnology. In *Tracking Environmental Change Using Lake Sediments*; Last, W.M., Smol, J.P., Eds.; Kluwer Academic Publishers: Dordrecht, The Netherlands, 2001; pp. 1–5. [CrossRef]
2. Roberts, N.; Jones, M.D.; Benkaddour, A.; Eastwood, W.J.; Filippi, M.L.; Frogley, M.R.; Lamb, H.F.; Leng, M.J.; Reed, J.M.; Stein, M.; et al. Stable Isotope Records of Late Quaternary Climate and Hydrology from Mediterranean Lakes: The ISOMED Synthesis. *Quat. Sci. Rev.* **2008**, *27*, 2426–2441. [CrossRef]
3. Mayewski, P.A.; Rohling, E.E.; Stager, J.C.; Karlén, W.; Maasch, K.A.; Meeker, L.D.; Meyerson, E.A.; Gasse, F.; van Kreveld, S.; Holmgren, K.; et al. Holocene Climate Variability. *Quat. Res.* **2004**, *62*, 243–255. [CrossRef]
4. Wanner, H.; Beer, J.; Bütikofer, J.; Crowley, T.J.; Cubasch, U.; Flückiger, J.; Goosse, H.; Grosjean, M.; Joos, F.; Kaplan, J.O.; et al. Mid- to Late Holocene Climate Change: An Overview. *Quat. Sci. Rev.* **2008**, *27*, 1791–1828. [CrossRef]
5. Ford, D.; Williams, P. *Karst Hydrogeology and Geomorphology*; John Wiley & Sons Ltd.: Chichester, UK, 2007.
6. Wolanski, E.; Brinson, M.; Cahoon, D.; Perillo, G. Coastal Wetlands: A Synthesis. In *Coastal Wetlands: An Integrated Ecosystem Approach*; Perillo, G., Wolanski, E., Cahoon, D., Brinson, M., Eds.; Elsevier Science: Amsterdam, The Netherlands, 2009; p. 64.
7. Pikelj, K.; Juračić, M. Eastern Adriatic Coast (EAC): Geomorphology and Coastal Vulnerability of a Karstic Coast. *J. Coast. Res.* **2013**, *289*, 944–957. [CrossRef]
8. Lambeck, K.; Antonioli, F.; Anzidei, M.; Ferranti, L.; Leoni, G.; Scicchitano, G.; Silenzi, S. Sea Level Change along the Italian Coast during the Holocene and Projections for the Future. *Quat. Int.* **2011**, *232*, 250–257. [CrossRef]
9. Vacchi, M.; Marriner, N.; Morhange, C.; Spada, G.; Fontana, A.; Rovere, A. Multiproxy Assessment of Holocene Relative Sea-Level Changes in the Western Mediterranean: Sea-Level Variability and Improvements in the Definition of the Isostatic Signal. *Earth Sci. Rev.* **2016**, *155*, 172–197. [CrossRef]
10. Schmidt, R.; Pugliese, N.; Müller, J.; Szeroczyriska, K.; Bogner, D.; Melis, R.; Kamenik, C.; Bari, A.; Danielopol, D.L. Palaeoclimate, Vegetation and Coastal Lake Development, from the Pleniglacial until Early Holocene, in the Northern Adriatic Valun Bay (Isle of Cres, Croatia). *Quat. Ital. J. Quat. Sci.* **2001**, *14*, 61–78.
11. Avramidis, P.; Iliopoulos, G.; Panagiotaras, D.; Papoulis, D.; Lambropoulou, P.; Kontopoulos, N.; Siavalas, G.; Christanis, K. Tracking Mid- to Late Holocene Depositional Environments by Applying Sedimentological, Palaeontological and Geochemical Proxies, Amvrakikos Coastal Lagoon Sediments, Western Greece, Mediterranean Sea. *Quat. Int.* **2014**, *332*, 19–36. [CrossRef]
12. Morellón, M.; Anselmetti, F.S.; Ariztegui, D.; Brushulli, B.; Sinopoli, G.; Wagner, B.; Sadori, L.; Gilli, A.; Pambuku, A. Human-Climate Interactions in the Central Mediterranean Region during the Last Millennia: The Laminated Record of Lake Butrint (Albania). *Quat. Sci. Rev.* **2016**, *136*, 134–152. [CrossRef]
13. Kaniewski, D.; Marriner, N.; Morhange, C.; Rius, D.; Carre, M.-B.; Faivre, S.; Van Campo, E. Croatia's Mid-Late Holocene (5200–3200 BP) Coastal Vegetation Shaped by Human Societies. *Quat. Sci. Rev.* **2018**, *200*, 334–350. [CrossRef]
14. Brunović, D.; Miko, S.; Ilijanić, N.; Peh, Z.; Hasan, O.; Kolar, T.; Miko, M.Š.; Razum, I. Holocene Foraminiferal and Geochemical Records in the Coastal Karst Dolines of Cres Island, Croatia. *Geol. Croat.* **2019**, *72*, 19–42. [CrossRef]
15. Brunović, D.; Miko, S.; Hasan, O.; Papatheodorou, G.; Ilijanić, N.; Miserocchi, S.; Correggiari, A.; Geraga, M. Late Pleistocene and Holocene Paleoenvironmental Reconstruction of a Drowned Karst Isolation Basin (Lošinj Channel, NE Adriatic Sea). *Palaeogeogr. Palaeoclimatol. Palaeoecol.* **2020**, *544*, 109587. [CrossRef]
16. Razum, I.; Miko, S.; Ilijanić, N.; Hasan, O.; Šparica Miko, M.; Brunović, D.; Pawlowsky-Glahn, V. A Compositional Approach to the Reconstruction of Geochemical Processes Involved in the Evolution of Holocene Marine Flooded Coastal Karst Basins (Mljet Island, Croatia). *Appl. Geochem.* **2020**, *116*, 104574. [CrossRef]
17. Razum, I.; Miko, S.; Ilijanić, N.; Petrelli, M.; Röhl, U.; Hasan, O.; Giaccio, B. Holocene Tephra Record of Lake Veliko Jezero, Croatia: Implications for the Central Mediterranean Tephrostratigraphy and Sea Level Rise. *Boreas* **2020**, *49*, 653–673. [CrossRef]
18. Wunsam, S.; Schmidt, R.; Müller, J. Holocene Lake Development of Two Dalmatian Lagoons (Malo and Veliko Jezero, Isle of Mljet) in Respect to Changes in Adriatic Sea Level and Climate. *Palaeogeogr. Palaeoclimatol. Palaeoecol.* **1999**, *146*, 251–281. [CrossRef]
19. Ilijanić, N. Minerali Glina u Jezerskim Sedimentima Istočno Jadranske Obale Kao Pokazatelji Promjena Okoliša Tijekom Kasnog Pleistocena i Holocena. Ph.D. Thesis, Faculty of Science, University of Zagreb, Zagreb, Croatia, 2014.
20. Marriner, N.; Morhange, C.; Faivre, S.; Flaux, C.; Vacchi, M.; Miko, S.; Dumas, V.; Boetto, G.; Radic Rossi, I. Post-Roman Sea-Level Changes on Pag Island (Adriatic Sea): Dating Croatia's "Enigmatic" Coastal Notch? *Geomorphology* **2014**, *221*, 83–94. [CrossRef]
21. Rossi, I.R. Underwater Cultural Heritage and Maritime Archaeology in Croatia: An Overview. *Eur. J. Archaeol.* **2012**, *15*, 285–308. [CrossRef]
22. Jerbić, K. Zambratija: A 6000-Year-Old Pile-Dwelling Submerged under the Adriatic Sea. Ph.D. Thesis, Flinders University, Bedford Park, Australia, 2020.
23. Bakrač, K.; Ilijanić, N.; Miko, S.; Hasan, O. Evidence of Sapropel S1 Formation from Holocene Lacustrine Sequences in Lake Vrana in Dalmatia (Croatia). *Quat. Int.* **2018**, *494*, 5–18. [CrossRef]
24. Galović, I.; Caput Mihalić, K.; Ilijanić, N.; Miko, S.; Hasan, O. Diatom Responses to Holocene Environmental Changes in a Karstic Lake Vrana in Dalmatia (Croatia). *Quat. Int.* **2018**, *494*, 167–179. [CrossRef]
25. Hajek-Tadesse, V.; Ilijanić, N.; Miko, S.; Hasan, O. Holocene Ostracoda (Crustacea) from the Shallow Lake Vrana (Dalmatia, Croatia) and Their Paleoenvironmental Significanc. *Quat. Int.* **2018**, *494*, 80–91. [CrossRef]

26. Ilijanić, N.; Miko, S.; Hasan, O.; Bakrač, K. Holocene Environmental Record from Lake Sediments in the Bokanjačko Blato Karst Polje (Dalmatia, Croatia). *Quat. Int.* **2018**, *494*, 66–79. [CrossRef]
27. Razum, I.; Bajo, P.; Brunović, D.; Ilijanić, N.; Hasan, O.; Röhl, U.; Miko, M.Š.; Miko, S. Past Climate Variations Recorded in Needle-like Aragonites Correlate with Organic Carbon Burial Efficiency as Revealed by Lake Sediments in Croatia. *Sci. Rep.* **2021**, *11*, 7568. [CrossRef] [PubMed]
28. Magny, M.; Peyron, O.; Sadori, L.; Ortu, E.; Zanchetta, G.; Vannière, B.; Tinner, W. Contrasting Patterns of Precipitation Seasonality during the Holocene in the South- and North-Central Mediterranean. *J. Quat. Sci.* **2012**, *27*, 290–296. [CrossRef]
29. Magny, M.; Combourieu-Nebout, N.; de Beaulieu, J.L.; Bout-Roumazeilles, V.; Colombaroli, D.; Desprat, S.; Francke, A.; Joannin, S.; Ortu, E.; Peyron, O.; et al. North–South Palaeohydrological Contrasts in the Central Mediterranean during the Holocene: Tentative Synthesis and Working Hypotheses. *Clim. Past* **2013**, *9*, 2043–2071. [CrossRef]
30. Peyron, O.; Magny, M.; Goring, S.; Joannin, S.; de Beaulieu, J.-L.; Brugiapaglia, E.; Sadori, L.; Garfi, G.; Kouli, K.; Ioakim, C.; et al. Contrasting Patterns of Climatic Changes during the Holocene across the Italian Peninsula Reconstructed from Pollen Data. *Clim. Past* **2013**, *9*, 1233–1252. [CrossRef]
31. Finné, M.; Woodbridge, J.; Labuhn, I.; Roberts, C.N. Holocene Hydro-Climatic Variability in the Mediterranean: A Synthetic Multi-Proxy Reconstruction. *Holocene* **2019**, *29*, 847–863. [CrossRef]
32. Seguin, J.; Avramidis, P.; Haug, A.; Kessler, T.; Schimmelmann, A.; Unkel, I. Reconstruction of Palaeoenvironmental Variability Based on an Inter- Comparison of Four Lacustrine Archives on the Peloponnese (Greece) for the Last 5000 Years. *EG Quat. Sci. J.* **2020**, *69*, 165–186. [CrossRef]
33. Roberts, N.; Eastwood, W.J.; Kuzucuoğlu, C.; Fiorentino, G.; Caracuta, V. Climatic, Vegetation and Cultural Change in the Eastern Mediterranean during the Mid-Holocene Environmental Transition. *Holocene* **2011**, *21*, 147–162. [CrossRef]
34. Piva, A.; Asioli, A.; Trincardi, F.; Schneider, R.R.; Vigliotti, L. Late-Holocene Climate Variability in the Adriatic Sea (Central Mediterranean). *Holocene* **2008**, *18*, 153–167. [CrossRef]
35. Combourieu-Nebout, N.; Peyron, O.; Bout-Roumazeilles, V.; Goring, S.; Dormoy, I.; Joannin, S.; Sadori, L.; Siani, G.; Magny, M. Holocene Vegetation and Climate Changes in the Central Mediterranean Inferred from a High-Resolution Marine Pollen Record (Adriatic Sea). *Clim. Past* **2013**, *9*, 2023–2042. [CrossRef]
36. Schmidt, R.; Müller, J.; Drescher-Schneider, R.; Krisai, R.; Szeroczyńska, K.; Barić, A. Changes in Lake Level and Trophy at Lake Vrana, a Large Karstic Lake on the Island of Cres (Croatia), with Respect to Palaeoclimate and Anthropogenic Impacts during the Last Approx. 16,000 Years. *J. Limnol.* **2000**, *59*, 113. [CrossRef]
37. Kaniewski, D.; Marriner, N.; Morhange, C.; Faivre, S.; Otto, T.; Van Campo, E. Solar Pacing of Storm Surges, Coastal Flooding and Agricultural Losses in the Central Mediterranean. *Sci. Rep.* **2016**, *6*, 25197. [CrossRef]
38. Siani, G.; Magny, M.; Paterne, M.; Debret, M.; Fontugne, M. Paleohydrology Reconstruction and Holocene Climate Variability in the South Adriatic Sea. *Clim. Past* **2013**, *9*, 499–515. [CrossRef]
39. Rudzka, D.; Mcdermott, F.; Surić, M. A Late Holocene Climate Record in Stalagmites from Modrič Cave (Croatia). *J. Quat. Sci.* **2012**, *27*, 585–596. [CrossRef]
40. Surić, M.; Bajo, P.; Lončarić, R.; Lončar, N.; Drysdale, R.N.; Hellstrom, J.C.; Hua, Q. Speleothem Records of the Hydroclimate Variability throughout the Last Glacial Cycle from Manita Peć Cave (Velebit Mountain, Croatia). *Geosciences* **2021**, *11*, 347. [CrossRef]
41. Lončar, N.; Bar-Matthews, M.; Ayalon, A.; Faivre, S.; Surić, M. Holocene Climatic Conditions in the Eastern Adriatic Recorded in Stalagmites from Strašna Peć Cave (Croatia). *Quat. Int.* **2019**, *508*, 98–106. [CrossRef]
42. Lončar, N.; Bar-Matthews, M.; Avalon, A.; Surić, M.; Faivre, S. Early and Mid-Holocene Environmental Conditions in the Eastern Adriatic Recorded in Speleotherms from Mala Špilja Cave and Velika Špilja Cave (Mljet Island, Croatia). *Acta Carsologica* **2017**, *46*, 229–249. [CrossRef]
43. Surić, M.; Columbu, A.; Lončarić, R.; Bajo, P.; Bočić, N.; Lončar, N.; Drysdale, R.N.; Hellstrom, J.C. Holocene Hydroclimate Changes in Continental Croatia Recorded in Speleothem δ 13 C and δ 18 O from Nova Grgosova Cave. *Holocene* **2021**, *31*, 1401–1416. [CrossRef]
44. Hasan, O. Paleookolišna Rekonstrukcija Slivova Karinskoga Mora, Novigradskoga Mora i Velebitskog Kanala Tijekom Holocena. Ph.D. Thesis, Faculty of Mining, Geology and Petroleum Engineering, University of Zagreb, Zagreb, Croatia, 2017.
45. Hasan, O.; Miko, S.; Brunović, D.; Papatheodorou, G.; Christodolou, D.; Ilijanić, N.; Geraga, M. Geomorphology of Canyon Outlets in Zrmanja River Estuary and Its Effect on the Holocene Flooding of Semi-Enclosed Basins (the Novigrad and Karin Seas, Eastern Adriatic). *Water* **2020**, *12*, 2807. [CrossRef]
46. Faivre, S.; Fouache, E.; Ghilardi, M.; Antonioli, F.; Furlani, S.; Kovačić, V. Relative Sea Level Change in Western Istria (Croatia) during the Last Millennium. *Quat. Int.* **2011**, *232*, 132–143. [CrossRef]
47. Felja, I.; Fontana, A.; Furlani, S.; Bajraktarević, Z.; Paradžik, A.; Topalović, E.; Rossato, S.; Ćosović, V.; Juračić, M. Environmental Changes in the Lower Mirna River Valley (Istria, Croatia) during Upper Holocene. *Geol. Croat.* **2015**, *68*, 209–224. [CrossRef]
48. Surić, M.; Juračić, M. Late Pleistocene—Holocene Environmental Changes—Records from Submerged Speleothems along the Eastern Adriatic Coast (Croatia). *Geol. Croat.* **2010**, *63*, 155–169. [CrossRef]
49. Surić, M.; Juračić, M.; Horvatinčić, N.; Krajcar Bronić, I. Late Pleistocene–Holocene Sea-Level Rise and the Pattern of Coastal Karst Inundation: Records from Submerged Speleothems along the Eastern Adriatic Coast (Croatia). *Mar. Geol.* **2005**, *214*, 163–175. [CrossRef]

50. Bechor, B.; Sivan, D.; Miko, S.; Hasan, O.; Grisonic, M.; Rossi, I.R.; Lorentzen, B.; Artioli, G.; Ricci, G.; Ivelja, T.; et al. Salt Pans as a New Archaeological Sea-Level Proxy: A Test Case from Dalmatia, Croatia. *Quat. Sci. Rev.* **2020**, *250*, 106680. [CrossRef]
51. Florido, E.; Auriemma, R.; Faivre, S.; Radić Rossi, I.; Antonioli, F.; Furlani, S.; Spada, G. Istrian and Dalmatian Fishtanks as Sea-Level Markers. *Quat. Int.* **2011**, *232*, 105–113. [CrossRef]
52. Ivelja, T.; Bechor, B.; Hasan, O.; Miko, S.; Sivan, D.; Brook, A. Improving Vertical Accuracy of Uav Digital Surface Models by Introducing Terrestrial Laser Scans on a Point-Cloud Level. *Int. Arch. Photogramm. Remote Sens. Spat. Inf. Sci* **2020**, *XLIII-B1-2*, 457–463. [CrossRef]
53. Faivre, S.; Bakran-Petricioli, T.; Horvatinčić, N.; Sironić, A. Distinct Phases of Relative Sea Level Changes in the Central Adriatic during the Last 1500 years—Influence of Climatic Variations? *Palaeogeogr. Palaeoclimatol. Palaeoecol.* **2013**, *369*, 163–174. [CrossRef]
54. Faivre, S.; Bakran-Petricioli, T.; Barešić, J.; Horvatić, D.; Macario, K. Relative Sea-Level Change and Climate Change in the Northeastern Adriatic during the Last 1.5 Ka (Istria, Croatia). *Quat. Sci. Rev.* **2019**, *222*, 105909. [CrossRef]
55. Fouache, E.; Faivre, S.; Glušček, S.; Kovačić, V.; Tassaux, F.; Dufaure, J.J. Evolution of the Croatian Shore Line between Poreč and Split over the Past 2000 Years. *Archaelogia Marit. Mediterr.* **2005**, *2*, 116–134.
56. Prohić, E.; Kniewald, G. Heavy Metal Distribution in Recent Sediments of the Krka River Estuary—An Example of Sequential Extraction Analysis. *Mar. Chem.* **1987**, *22*, 279–297. [CrossRef]
57. Bogner, D.; Juracic, M.; Odžak, N.; Baric, A. Trace Metals in Fine Grained Sediments of the Kaštela Bay, Adriatic Sea. *Water Sci. Technol.* **1998**, *38*, 169–175. [CrossRef]
58. Šparica, M.; Koch, G.; Belak, M.; Miko, S.; Šparica Miko, M.; Viličić, D.; Dolenec, T.; Bergant, S.; Lojen, S.; Vreča, P.; et al. Recent Sediments of Makirina Bay (Northern Dalmatia, Croatia): Their Origin Viewed through a Multidisciplinary Approach. *Geol. Croat.* **2005**, *58*, 21–71.
59. Miko, S.; Koch, G.; Mesić, S.; Šparica Miko, M.; Šparica, M.; Vreča, P.; Dolenec, T. Influence of Land Use in Small Karst Watersheds on the Chemical Status of Peloid Sediments on the Eastern Adriatic Coast. *J. Soils Sediments* **2007**, *7*, 303–312. [CrossRef]
60. Sondi, I.; Lojen, S.; Juračić, M.; Prohić, E. Mechanisms of Land–Sea Interactions—The Distribution of Metals and Sedimentary Organic Matter in Sediments of a River-Dominated Mediterranean Karstic Estuary. *Estuar. Coast. Shelf Sci.* **2008**, *80*, 12–20. [CrossRef]
61. Cuculić, V.; Cukrov, N.; Kwokal, Ž.; Mlakar, M. Natural and Anthropogenic Sources of Hg, Cd, Pb, Cu and Zn in Seawater and Sediment of Mljet National Park, Croatia. *Estuar. Coast. Shelf Sci.* **2009**, *81*, 311–320. [CrossRef]
62. Cukrov, N.; Frančišković-Bilinski, S.; Hlača, B.; Barišić, D. A Recent History of Metal Accumulation in the Sediments of Rijeka Harbor, Adriatic Sea, Croatia. *Mar. Pollut. Bull.* **2011**, *62*, 154–167. [CrossRef] [PubMed]
63. Obhođaš, J.; Valković, V.; Matjačić, L.; Nađ, K.; Sudac, D. Evaluation of Elemental Composition of Sediments from the Adriatic Sea by Using EDXRF Technique. *Appl. Radiat. Isot.* **2012**, *70*, 1392–1395. [CrossRef]
64. Lovrenčić Mikelić, I.; Oreščanin, V.; Barišić, D. Distribution and Origin of Major, Minor, and Trace Elements in Sediments and Sedimentary Rocks of the Kaštela Bay (Croatia) Coastal Area. *J. Geochem. Explor.* **2013**, *128*, 1–13. [CrossRef]
65. Ivanić, M.; Lojen, S.; Grozić, D.; Jurina, I.; Škapin, S.D.; Troskot-Čorbić, T.; Mikac, N.; Juračić, M.; Sondi, I. Geochemistry of Sedimentary Organic Matter and Trace Elements in Modern Lake Sediments from Transitional Karstic Land-Sea Environment of the Neretva River Delta (Kuti Lake, Croatia). *Quat. Int.* **2018**, *494*, 286–299. [CrossRef]
66. Cukrov, N.; Doumandji, N.; Garnier, C.; Tucaković, I.; Dang, D.H.; Omanović, D.; Cukrov, N. Anthropogenic Mercury Contamination in Sediments of Krka River Estuary (Croatia). *Environ. Sci. Pollut. Res.* **2020**, *27*, 7628–7638. [CrossRef]
67. Dolenec, T.; Faganeli, J.; Pirc, S. Major, Minor and Trace Elements in Surficial Sediments from the Open Adriatic Sea: A Regional Geochemical Study. *Geol. Croat.* **1998**, *51*, 59–73.
68. De Lazzari, A.; Rampazzo, G.; Pavoni, B. Geochemistry of Sediments in the Northern and Central Adriatic Sea. *Estuar. Coast. Shelf Sci.* **2004**, *59*, 429–440. [CrossRef]
69. Spagnoli, F.; Dell'Anno, A.; De Marco, A.; Dinelli, E.; Fabiano, M.; Gadaleta, M.V.; Ianni, C.; Loiacono, F.; Manini, E.; Marini, M.; et al. Biogeochemistry, Grain Size and Mineralogy of the Central and Southern Adriatic Sea Sediments: A Review. *Chem. Ecol.* **2010**, *26*, 19–44. [CrossRef]
70. Calanchi, N.; Dinelli, E.; Lucchini, F.; Mordenti, A. Chemostratigraphy of Late Quaternary Sediments from Lake Albano and Central Adriatic Sea Cores (PALICLAS Project). *Mem. dell'Istituto Ital. Idrobiol.* **1996**, *55*, 247–263.
71. Kelletat, D.H. Dalmatian Coasts. In *Encyclopedia of Coastal Science*; Schwartz, M., Ed.; Springer: Dordrecht, The Netherlands, 2005; pp. 355–356. [CrossRef]
72. Leder, T.D.; Ujević, T.; Čala, M. Coastline Lenghts and Areas of Islands in the Croatian Part of the Adriatic Sea Determined from the Topographic Maps at the Scale of 1:25,000. *Geoadria* **2017**, *9*, 5–32. [CrossRef]
73. Vlahović, I.; Tišljar, J.; Velić, I.; Matičec, D. Evolution of the Adriatic Carbonate Platform: Palaeogeography, Main Events and Depositional Dynamics. *Palaeogeogr. Palaeoclimatol. Palaeoecol.* **2005**, *220*, 333–360.
74. Mamužić, P.; Sokač, B.; Velić, I. *Osnovna Geološka Karta SFRJ 1:100,000, List Silba*; Institut za Geološka Istraživanja: Zagreb, Croatia, 1970.
75. Mamužić, P.; Sokač, B. *Osnovna Geološka Karta SFRJ 1:100,000. Tumač Za Listove Molat i Silba*; Institut za Geološka Istraživanja: Zagreb, Croatia, 1973; p. 45.
76. Sokač, B.; Nikler, I.; Velić, I.; Mamužić, P. *Osnovna Geološka Karta SFRJ, 1:100,000, List Gospić*; Institut za Geološka Istraživanja: Zagreb, Croatia, 1974.

77. Sokač, B.; Ščavničar, B.; Velić, I. *Osnovna Geološka Karta SFRJ, 1:100,000. Tumač Za List Gospić*; Institut za Geološka Istraživanja: Zagreb, Croatia, 1976; p. 64.
78. Bulić, J.; Jurišić-Polšak, Z. Macropalaeontology and Stratigraphy of Lacustrine Miocene Deposits at Crnika Beach on the Island of Pag (Croatia). *Geol. Croat.* **2009**, *62*, 135–156. [CrossRef]
79. Jiménez-Moreno, G.; de Leeuw, A.; Mandic, O.; Harzhauser, M.; Pavelić, D.; Krijgsman, W.; Vranjković, A. Integrated Stratigraphy of the Early Miocene Lacustrine Deposits of Pag Island (SW Croatia): Palaeovegetation and Environmental Changes in the Dinaride Lake System. *Palaeogeogr. Palaeoclimatol. Palaeoecol.* **2009**, *280*, 193–206. [CrossRef]
80. Magdalenić, A. Hidrogeologija Otoka Paga. *Krš Jugosl.* **1984**, *10–16*, 119–137.
81. Lukač Reberski, J.; Terzić, J.; Dolić, S. Hydrogeological and Hydrochemical Features of the Island of Pag. In Proceedings of the 4th Croatian Geological Congress, Zagreb, Croatia, 14–15 October 2010; pp. 209–210.
82. Ljubešić, J.; Munda, B. *Elaborat Zona Sanitarne Zaštite Vodocrpilište Velo blato—Otok Pag*; Documentation fund Croatian Waters: Zagreb, Croatia, 2015.
83. Faričić, J. Pag Island on Old Cartographic Presentations. *Geoadria* **2003**, *8*, 47–126. (In Croatian) [CrossRef]
84. Sinergise Ltd. EO Browser. Available online: https://apps.sentinel-hub.com/eo-browser/ (accessed on 8 August 2021).
85. Lončar, N. Geomorphologic Regionalization of the Central and Southern Parts of Pag Island. *Geoadria* **2009**, *14*, 5–25. [CrossRef]
86. Mitić, B.; Topić, J.; Ilijanić, L.; Jasprica, N.; Milović, M.; Ruščić, M.; Pandža, M.; Bogdanović, S.; Dolina, K. *Kartiranje Flore Dalmacije, Prioritetna Područja: Otok Pag, Estuarij Krke, Otok Vis i Pučinski Otoci, Pelješac i Mljet, Tok Cetine*; Final report ver. 3; Faculty of Science, University of Zagreb: Zagreb, Croatia, 2009.
87. Blott, S.J.; Pye, K. GRADISTAT: A Grain Size Distribution and Statistics Package for the Analysis of Unconsolidated Sediments. *Earth Surf. Process Landforms* **2001**, *26*, 1237–1248. [CrossRef]
88. Moore, D.M.; Reynolds, R.C. *X-Ray Diffraction and the Identification and Analysis of Clay Minerals*, 2nd ed.; Oxford University Press: Oxford, UK, 1997.
89. Van der Weijden, C.H. Pitfalls of Normalization of Marine Geochemical Data Using a Common Divisor. *Mar. Geol.* **2002**, *184*, 167–187. [CrossRef]
90. Karageorgis, A.P.; Katsanevakis, S.; Kaberi, H. Use of Enrichment Factors for the Assessment of Heavy Metal Contamination in the Sediments of Koumoundourou Lake, Greece. *Water. Air. Soil Pollut.* **2009**, *204*, 243–258. [CrossRef]
91. Migani, F.; Borghesi, F.; Dinelli, E. Geochemical Characterization of Surface Sediments from the Northern Adriatic Wetlands around the Po River Delta. Part I: Bulk Composition and Relation to Local Background. *J. Geochem. Explor.* **2015**, *156*, 72–88. [CrossRef]
92. Ridgway, J.; Shimmield, G. Estuaries as Repositories of Historical Contamination and Their Impact on Shelf Seas. *Estuar. Coast. Shelf Sci.* **2002**, *55*, 903–928. [CrossRef]
93. Zhang, L.; Ye, X.; Feng, H.; Jing, Y.; Ouyang, T.; Yu, X.; Liang, R.; Gao, C.; Chen, W. Heavy Metal Contamination in Western Xiamen Bay Sediments and Its Vicinity, China. *Mar. Pollut. Bull.* **2007**, *54*, 974–982. [CrossRef]
94. Fuhrmann, R. *Atlas Quartärer Und Rezenter Ostrakoden Mitteldeutschlands*; Altenburger Naturwissenschaftliche Forschungen: Altenburg, Germany, 2012.
95. Meisch, C. *Freshwater Ostracoda of Western and Central Europe*; Spektrum Akademischer Verlag: Heidelberg, Germany, 2000.
96. Reimer, P.J.; Austin, W.E.N.; Bard, E.; Bayliss, A.; Blackwell, P.G.; Bronk Ramsey, C.; Butzin, M.; Cheng, H.; Edwards, R.L.; Friedrich, M.; et al. The IntCal20 Northern Hemisphere Radiocarbon Age Calibration Curve (0-55 Cal KBP). *Radiocarbon* **2020**, *62*, 725–757. [CrossRef]
97. Heaton, T.J.; Köhler, P.; Butzin, M.; Bard, E.; Reimer, R.W.; Austin, W.E.N.; Bronk Ramsey, C.; Grootes, P.M.; Hughen, K.A.; Kromer, B.; et al. Marine20—The Marine Radiocarbon Age Calibration Curve (0-55,000 Cal BP). *Radiocarbon* **2020**, *62*, 779–820. [CrossRef]
98. Folk, R.L.; Ward, W.C. Brazos River Bar [Texas]; a Study in the Significance of Grain Size Parameters. *J. Sediment. Res.* **1957**, *27*, 3–26. [CrossRef]
99. Hu, Q.-H.; Weng, J.-Q.; Wang, J.-S. Sources of Anthropogenic Radionuclides in the Environment: A Review. *J. Environ. Radioact.* **2010**, *101*, 426–437. [CrossRef] [PubMed]
100. Jurina, I.; Ivanić, M.; Troskot-Čorbić, T.; Barišić, D.; Vdović, N.; Sondi, I. Activity Concentrations and Distribution of Radionuclides in Surface and Core Sediments of the Neretva Channel (Adriatic Sea, Croatia). *Geol. Croat.* **2013**, *66*, 143–150. [CrossRef]
101. Fajkovic, H.; Lovrencic Mikelic, I.; Prohic, E. Vertical Distribution of 40K, 232Th, and 137Cs Mass Activities in Lake Sediment (Vransko Lake, Croatia) and Their Relationship with the Source Material and Sedimentation. *J. Radioanal. Nucl. Chem.* **2013**, *295*, 2273–2282. [CrossRef]
102. Horvatinčić, N.; Sironić, A.; Barešić, J.; Bronić, I.; Nikolov, J.; Todorović, N.; Hansman, J.; Krmar, M. Isotope Analyses of the Lake Sediments in the Plitvice Lakes, Croatia. *Open Phys.* **2014**, *12*, 707–713. [CrossRef]
103. Miko, S.; Hasan, O.; Ilijanić, N.; Razum, I. Final Report of RV Poseidon Scientific Cruise POS514; Zagreb, Croatia. 2019. Available online: https://www.bib.irb.hr/1029618 (accessed on 22 December 2021).
104. Petrinec, B.; Franic, Z.; Ilijanic, N.; Miko, S.; Strok, M.; Smodis, B. Estimation of Sedimentation Rate in the Middle and South Adriatic Sea Using 137Cs. *Radiat. Prot. Dosim.* **2012**, *151*, 102–111. [CrossRef]
105. Cukrov, N.; Barišić, D.; Juračić, M. Calculated Sedimentation Rate in the Krka River Estruary Using Vertical Diostribution of 137Cs. *CIESM Congr. Rapp. Comm. Int. Mer. Médit.* **2007**, *38*, 81.

106. Lambeck, K.; Rouby, H.; Purcell, A.; Sun, Y.; Sambridge, M. Sea Level and Global Ice Volumes from the Last Glacial Maximum to the Holocene. *Proc. Natl. Acad. Sci. USA* **2014**, *111*, 15296–15303. [CrossRef]
107. Antonioli, F.; Ferranti, L.; Fontana, A.; Amorosi, A.; Bondesan, A.; Braitenberg, C.; Dutton, A.; Fontolan, G.; Furlani, S.; Lambeck, K.; et al. Holocene Relative Sea-Level Changes and Vertical Movements along the Italian and Istrian Coastlines. *Quat. Int.* **2009**, *206*, 102–133. [CrossRef]
108. Rogić, V. Regional-Geographical Aspect of the Pag Commune. *Geogr. Glas.* **1972**, *33–34*, 141–157. (In Croatian)
109. Correggiari, A.; Roveri, M.; Trincardi, F. Late Pleistocene and Holocene Evolution of the North Adriatic Sea. *Quat. Ital. J. Quat. Sci.* **1996**, *9*, 697–704.
110. Benjamin, J.; Rovere, A.; Fontana, A.; Furlani, S.; Vacchi, M.; Inglis, R.H.; Galili, E.; Antonioli, F.; Sivan, D.; Miko, S.; et al. Late Quaternary Sea-Level Changes and Early Human Societies in the Central and Eastern Mediterranean Basin: An Interdisciplinary Review. *Quat. Int.* **2017**, *449*, 29–57. [CrossRef]
111. Håkanson, L.; Jansson, M. *Principles of Lake Sedimentology*; The Blackburn Press: Caldwell, NJ, USA, 2002.
112. Boomer, I.; Horne, D.J.; Slipper, I.J. Boomer, Horne, Slipper (2013)_The Use of Ostracods in Palaeoenvironmental Studies. *Paleontol. Soc. Pap.* **2003**, *9*, 153–180. [CrossRef]
113. Lord, A.R.; Boomer, I.; Brouwers, E.; Whittaker, J.E. Ostracod Taxa as Palaeoclimate Indicators in the Quaternary. In *Ostracoda as Proxies for Quaternary Climate Change*; Horne, D.J., Holmes, J.A., Rodriguez-Lazaro, J., Viehberg, F.A., Eds.; Elsevier: Oxford, UK, 2012; pp. 37–45.
114. Meyers, P.A.; Teranes, J.L. Sediment Organic Matter. In *Tracking Environmental Change Using Lake Sediments Vol. 2: Physical and Geochemical Methods*; Last, W.M., Smol, J.P., Eds.; Kluwer Academic Publisher: Dordrecht, The Netherlands, 2001; pp. 239–269.
115. Meyers, P.A. Applications of Organic Geochemistry to Paleolimnological Reconstructions: A Summary of Examples from the Laurentian Great Lakes. *Org. Geochem.* **2003**, *34*, 261–289. [CrossRef]
116. Frenzel, P.; Boomer, I. The Use of Ostracods from Marginal Marine, Brackish Waters as Bioindicators of Modern and Quaternary Environmental Change. *Palaeogeogr. Palaeoclimatol. Palaeoecol.* **2005**, *225*, 68–92. [CrossRef]
117. Marco-Barba, J.; Mesquita-Joanes, F.; Miracle, M. Ostracod Palaeolimnological Analysis Reveals Drastic Historical Changes in Salinity, Eutrophication and Biodiversity Loss in a Coastal Mediterranean Lake. *Holocene* **2013**, *23*, 556–567. [CrossRef]
118. Curry, B.; Henne, P.D.; Mesquita-Joanes, F.; Marrone, F.; Pieri, V.; La Mantia, T.; Calò, C.; Tinner, W. Holocene Paleoclimate Inferred from Salinity Histories of Adjacent Lakes in Southwestern Sicily (Italy). *Quat. Sci. Rev.* **2016**, *150*, 67–83. [CrossRef]
119. Griffiths, H.I.; Holmes, J.A. *Non-Marine Ostracods and Quaternary Palaeoenvironments*; Quaternary Research Association: London, UK, 2000; p. 179.
120. Terzić, J.; Peh, Z.; Marković, T. Hydrochemical Properties of Transition Zone between Fresh Groundwater and Seawater in Karst Environment of the Adriatic Islands, Croatia. *Environ. Earth Sci.* **2010**, *59*, 1629–1642. [CrossRef]
121. Terzić, J.; Grgec, D.; Lukač Reberski, J.; Selak, A.; Boljat, I.; Filipović, M. Hydrogeological Estimation of Brackish Groundwater Lens on a Small Dinaric Karst Island: Case Study of Ilovik, Croatia. *CATENA* **2021**, *204*, 105379. [CrossRef]
122. Ghyben, W.B. *Nota in Verband Met de Voorgenomen Putboring Nabij Amsterdam*; Tijdschrift van Let Koninklijk Instituut van Ingenieurs: The Hague, The Netherlands, 1888.
123. Herzberg, A. Die Wasserversorgung Einiger Nordseebader. *Wasserversorgung* **1901**, *44*, 815–844, 815–819, 842–844.
124. Mann, M.E.; Zhang, Z.; Rutherford, S.; Bradley, R.S.; Hughes, M.K.; Shindell, D.; Ammann, C.; Faluvegi, G.; Ni, F. Global Signatures and Dynamical Origins of the Little Ice Age and Medieval Climate Anomaly. *Science* **2009**, *326*, 1256–1260. [CrossRef]
125. Marcott, S.A.; Shakun, J.D.; Clark, P.U.; Mix, A.C. A Reconstruction of Regional and Global Temperature for the Past 11,300 Years. *Science* **2013**, *339*, 1198–1201. [CrossRef] [PubMed]
126. Francke, A.; Wagner, B.; Leng, M.J.; Rethemeyer, J. A Late Glacial to Holocene Record of Environmental Change from Lake Dojran (Macedonia, Greece). *Clim. Past* **2013**, *9*, 481–498. [CrossRef]
127. Thienemann, M.; Masi, A.; Kusch, S.; Sadori, L.; John, S.; Francke, A.; Wagner, B.; Rethemeyer, J. Organic Geochemical and Palynological Evidence for Holocene Natural and Anthropogenic Environmental Change at Lake Dojran (Macedonia/Greece). *Holocene* **2017**, *27*, 1103–1114. [CrossRef]
128. Curry, B.B.; Filippelli, G.M. Episodes of Low Dissolved Oxygen Indicated by Ostracodes and Sediment Geochemistry at Crystal Lake, Illinois, USA. *Limnol. Oceanogr.* **2010**, *55*, 2403–2423. [CrossRef]
129. Jahn, A.; Gamenick, I.; Theede, H. Physiological Adaptations of Cyprideis torosa (Crustacea, Ostracoda) to Hydrogen Sulphide. *Mar. Ecol. Prog. Ser.* **1996**, *142*, 215–223. [CrossRef]
130. Ligero, R.; Ramos-Lerate, I.; Barrera, M.; Casas-Ruiz, M. Relationships between Sea-Bed Radionuclide Activities and Some Sedimentological Variables. *J. Environ. Radioact.* **2001**, *57*, 7–19. [CrossRef]
131. Rubio, L.; Linares-Rueda, A.; Dueñas, C.; Fernández, M.C.; Clavero, V.; Niell, F.X.; Fernández, J.A. Sediment Accumulation Rate and Radiological Characterisation of the Sediment of Palmones River Estuary (Southern of Spain). *J. Environ. Radioact.* **2003**, *65*, 267–280. [CrossRef]
132. Halamić, J.; Peh, Z.; Miko, S.; Galović, L.; Šorša, A. Geochemical Atlas of Croatia: Environmental Implications and Geodynamical Thread. *J. Geochem. Explor.* **2012**, *115*, 36–46. [CrossRef]
133. Mateo, R. Lead poisoning in wild birds in Europe and the regulations adopted by different countries. In *Ingestion of Lead from Spent Ammunition: Implications for Wildlife and Humans*; Watson, R.T., Fuller, M., Pokras, M., Hunt, W.G., Eds.; The Peregrine Fund: Boise, ID, USA, 2009. [CrossRef]

134. Jurina, I.; Ivanić, M.; Vdović, N.; Troskot-Čorbić, T.; Lojen, S.; Mikac, N.; Sondi, I. Deposition of Trace Metals in Sediments of the Deltaic Plain and Adjacent Coastal Area (the Neretva River, Adriatic Sea). *J. Geochem. Explor.* **2015**, *157*, 120–131. [CrossRef]
135. Kwokal, Ž.; Frančišković-Bilinski, S.; Bilinski, H.; Branica, M. A Comparison of Anthropogenic Mercury Pollution in Kaštela Bay (Croatia) with Pristine Estuaries in Öre (Sweden) and Krka (Croatia). *Mar. Pollut. Bull.* **2002**, *44*, 1152–1157. [CrossRef]